BLANK PAGE

NAVY DEPARTMENT
BUREAU OF ORDNANCE
WASHINGTON 25, D. C.

Vice Admiral G.F. Hussey, Jr., USN
Chief of the Bureau of Ordnance

Captain K.H. Noble, USN
Director, Research and
Development Division

Commander J.I. Cone, USN
Ammunition and Explosives

Commander Stephen Brunauer, USNR
High Explosives and Amphibious
Demolition Munitions

Research Group in Theoretical Physics

NAVORD Report 69-46

INTERFEROMETRIC STUDY OF SUPERSONIC PHENOMENA

Part I
A Supersonic Air Jet at 60 LB/IN^2 Tank Pressure

R. Ladenburg, C. C. Van Voorhis, and J. Winckler

Palmer Physical Laboratory
Princeton University
Princeton, New Jersey

17 April 1946

NAVY DEPARTMENT
BUREAU OF ORDNANCE
WASHINGTON 25, D. C.

17 April 1946

NAVORD REPORT 69-46

INTERFEROMETRIC STUDY OF SUPERSONIC PHENOMENA, Part I: A Supersonic Air Jet at 60 LB/IN^2 Tank Pressure

1. NAVORD Report 69-46 presents data on the interferometric studies of supersonic phenomena and is the first of a series of reports on this subject published for the use of agencies conducting explosives research.

2. This report presents preliminary data and therefore does not constitute a final comprehensive study. Additional information and criticism by other agencies for incorporation in future reports is requested.

3. The findings herein represent the interpretations of the authors and are not necessarily the views of the Bureau of Ordnance. The work has been done under contract NOrd 9240 at the Palmer Physical Laboratory at Princeton University. The BuOrd liaison officers are Dr. R. J. Seeger and Dr. F. J. Weyl.

4. This report does not supersede any existing publication.

G. F. HUSSEY, JR.
Vice Admiral, U. S. Navy
Chief of the Bureau of Ordnance

Captain, U. S. Navy
Director, Research and
Development Division
By direction

PREFACE

The work to be described in the present and in subsequent reports on interferometric studies of supersonic phenomena originated in discussions between Drs. R. Ladenburg and J. Von Neumann on the behavior of propellant gases expanding from guns. Dr. Von Neumann proposed the application of interferometric methods to the study of such phenomena, and at his suggestion, the Bureau of Ordnance requested the Coordinator of Research and Development of the Navy Department to initiate a project on the interferometric examination of air jets and related phenomena with the National Defense Research Committee of the Office of Scientific Research and Development. Consequently, such a project was set up at the Princeton Station of Division 2 of the National Defense Research Committee under the direction of R. Ladenburg. In June, 1945, the Bureau of Ordnance took over this work directly under contract NOrd 9240.

The first experiments were carried out with a Jamin-Mach type interferometer constructed and used before by Ladenburg and collaborators. Inasmuch as the preliminary results obtained on the air jet from a commercial pressure tank released through a straight tube were quite successful,[1] an interferometer of the Zehnder-Mach type, more suitable for the planned study, was constructed. The necessary plane-parallel plates and plane mirrors were obtained by loan from Dr. R. B. Kennard of the

1) See Report on Project No. 208, Princeton University Station, Division 2, NDRC (dated May 15, 1944) "Study of Shock Waves by Interferometry" by R. Ladenburg and C. C. Van Voorhis.

National Bureau of Standards, and under his supervision the supports of the plates with fine adjustments were manufactured by the machine shop of the National Bureau of Standards in the summer of 1944. The plates have a size of 30 x 60 mm and, although not perfect, have proved to be very valuable and have been used for the various experiments carried out.

This interferometer was installed in an annex to Palmer Physics Laboratory at ground level on concrete foundations and insulated by rubber cushions against vibrations. The gas jet to be studied emerges from a large pressure tank of about 1.5 cubic meter capacity, through a 1 inch tube ending in orifices of various forms. The jet is produced by quickly opening a special valve. The tank and the tube are installed in such a way that the jet crosses one beam of the interferometer and that the surface of the orifice is slightly above the plane through the lower edges of the interferometer plates. Details of the outlay, of the light source used, of the photographic equipment, etc., are given in later sections of the present report.

Preliminary experiments with a nitrogen jet at 44 lb./in^2 tank pressure have been described in a second report[2] and experiments with an air jet at tank pressure of 60 lb./in^2 were described in a third report of Division 2, N.D.R.C.[3] Also the analysis of the interferograms obtained and the computation of density, pressure, temperature and gas velocity at various

2) Monthly Report AES-5 (OSRD-4514) Project No. 208, OD-03 (dated December 25, 1944).

3) OSRD Report No. A-332
NDRC Report No. 5204.

points in the jet, including the shock region, are given in this report.

Using this equipment a large series of experiments at various pressures of the tank filled with compressed air between 20 and 100 lbs./in^2 have been carried out and evaluated by improved methods. In most cases a streamlined orifice has been used. Shock strength - that is the ratio of the pressures on both sides of a shock - up to 11 and Mach numbers up to 4 have been obtained. The results were compared with the conventional theory of compressible nonviscous fluids and, in general, good agreement was obtained. Interesting relations between the densities for different pressures at corresponding distances from the orifice were revealed.

In another series of experiments a carefully designed Laval nozzle was attached to the one-inch tube replacing the streamlined orifice. In this way a homogeneous cylindrical jet was obtained containing a shock free region of constant Mach number 1.70. Conical objects of various cone angles, a caliber .30 projectile and a sphere of 5/16" diameter were supported in this "open wind tunnel" and the distributions of density, pressure, etc. around these objects were determined from the interferograms obtained. The results obtained with the cone of 30° half angle have been compared quantitatively with the theory of Taylor-Maccoll.

In the course of these experiments the project was transferred from the Office of Scientific Research and Development to the Bureau of Ordnance, Navy Department, as sponsor.

The present report, the first of a longer series, contains a discussion of the Mach Interferometer and of the technique of adjusting the instrument, the method for analyzing interferograms, the analysis of a supersonic jet from a 10 mm streamlined orifice at 60 lb./in^2 tank pressure and the comparison of the results obtained with the conventional aerodynamical theory.

The experiments and results with 20, 30, 40, 60, 80 and 100 lbs. in the tank and the relations between the results at different pressures will be given in a second report.

A third one will contain the studies of the homogeneous jet of constant Mach number and of the distribution of density, pressure, etc around the various objects inserted in this "open wind tunnel."

The present work has been carried out jointly by R. Ladenburg, C. C. Van Voorhis and J. Winckler with the assistance of Mr. H. Panofsky for some of the work. A large part of the experimental technique is due to Mr. Winckler. In the laborious computations the skilled technique of Miss A. Kenney was of great help.

ABSTRACT

The present report is the first of a series describing optical, especially interferometric studies, of supersonic phenomena. After a general survey of the literature and of the various optical methods of studying gas flow a discussion of a Zehnder-Mach interferometer is given, showing the way fringes are produced, and the effect of various fringe widths and orientations. Errors from refraction and nonparallel light are shown to be negligible. A technique of adjusting the interferometer is described in detail. Also various auxiliary apparatus is discussed.

The method for analyzing interferograms is given, describing how the fringe shifts are obtained and how the density is evaluated in cases of circular symmetry of the jet.

A supersonic air jet from a 10-mm diameter streamlined orifice at 60 lb./in^2 tank pressure has been analyzed, using much improved experimental techniques. Pressures, temperatures, Mach numbers, and velocities have been calculated from the density values in the jet and the initial conditions. Shock strengths, entropy changes, and conditions at the orifice and slip stream are found generally in good agreement with theory.

List of Figures

List of Tables

BLANK PAGE

INTERFEROMETRIC STUDY OF SUPERSONIC PHENOMENA
Part I:
A Supersonic Air Jet at 60 LB/IN^2 Tank Pressure

I. HISTORICAL SURVEY

The study of the flow of gases from a reservoir through an orifice into a receiver dates back to the original work of St. Venant and Wantzel (1)* more than a century ago. The existing knowledge of the compressible flow of gases through pipes and orifices is summarized in several publications (2).

A significant advance was made by Osborne Reynolds, who discovered in 1885 (3) that if the ratio of the receiver to reservoir pressure drops below a certain critical value (P/P_o = .527 for a perfect diatomic gas) the velocity of the gas at the narrowest part of the passage reaches the local velocity of sound, and up to the point of reaching the constriction the flow is unaffected by the receiver conditions. If the orifice through which the gas emerges into the receiver is the narrowest part of the system, a free gas jet flowing at sound velocity at the orifice is formed. Then if the pressure ratio P/P_o is lower than the critical value, the jet expands into the receiver, attaining supersonic velocity. In such supersonic jets stationary patterns, consisting of expansions and constrictions accompanied by shock waves[4]/ appear, under

*Numbers in parenthesis refer to the list of references at the end of the report.

4/ The shocks, or discontinuities in the density, pressure, temperature and velocity of the air in the jet are fundamentally the same as those arising from an explosion. A bibliography of the more important works in this field is given in reference (21).

certain conditions repeating themselves many times as the jet proceeds out from the orifice.

Since this is the most prominent feature of such jets it was the first to be studied, originally by E. Mach and Salcher (4), and later by Emden (5), by means of the schlieren and shadowgraph technique. Theoretical explanations for the periodic structure were made by Prandtl (6), Von Karman (7), and Lord Rayleigh (8). An account of the mathematical ideas involved (especially those of Rayleigh) and a bibliography on the subject is given by Bateman (reference 2-B, para. 2.4).

Such derivations assume that the gas velocity normal to the jet direction is small, or, in other words, that the jet expands very little, its pressure being about the same as the receiver, and that conditions throughout the jet are nearly constant. The adiabatic law, or the existence of a velocity potential is also assumed throughout the flow. Under these assumptions a wavelength, λ , representing the distance between the successive "discs" or periods of expansion and contraction as shown in Mach and Emden's photographs is obtained, in more or less agreement with some of the experiments. These derivations are certainly not applicable when the jet undergoes an appreciable radial expansion. Also, the existence of standing discontinuities which make the flow non-isentropic, and the turbulent mixing of the jet stream with the surrounding air, along with the other effects of viscosity and heat conduction, are neglected in these treatments.

Hartman and Lazarus (13) have made the most recent investigation in which values of λ were measured, and they give emperical formulae which differ, especially at high pressures, from the theoretical equations.

It is evident that the flow of the gas in such jets does not, in general, possess the simple properties assumed in this type of theory, and more knowledge, both theoretical and experimental, must be forthcoming before a general treatment which holds over a wide range of pressure and expansion ratios can be made.

The proper approach to the subject would seem to be to study in detail the structure of only the first section, or period, and such is the purpose of the present work. L. Mach (9) made such a study in some detail qualitatively, using schlieren and interferometric techniques for the optical examination. He showed that standing "sound" waves of conical shape similar to those observed ahead of a projectile in flight existed in the jet, and that these waves could be reflected with change of phase at the free boundary between the jet and the atmosphere due to the sudden change in velocity of the gas at this point. Furthermore, at low reservoir pressure he showed that these "sound" waves intersected in a simple way to form an X but at higher pressures they became stronger and a flat wave normal to the stream appeared Y This he interpreted as the same kind of interaction observed and studied in detail earlier by E. Mach (10) when two

explosion waves collided, or when an explosion wave was reflected from a surface. This point will be discussed in more detail in later reports. L. Mach also found from a rough quantitative evaluation of the interference photographs that the air density in the jet at emergence was in general higher than that of the atmosphere, but that at distances out from the orifice the density dropped far below atmospheric density in many cases.

Cranz and Glatzel (11) made a study of jets at very high pressures formed by the ejection of powder gases from an 8 mm gun. They measured the Mach number distribution with probes and made shadowgrams of the shock formations. It has recently been shown in connection with the present work that tnese velocity measurements are in error, however, due to boundary layer phenomena (see Part VI-7). W. Pupp, working in Cranz's laboratory, made what is probably the first quantitative evaluation of the density in a supersonic jet by interferometry. This is described in Cranz's "Ballistik" Vol. II, page 192, but in insufficient detail for comparison with the present study, as only axial pressure values are given.

Stanton (12) investigated certain properties of jets, particularly the conditions just at the orifice, by using static pressure sounds and pitot tubes. He determined the exact position of the minimum cross section, the effect of scaling, and measured the pressure distribution on the axis of the jet. His results are not complete enough to determine the flow pattern and shockwave formation of the jet, however.

His values of P/P_o were in the vicinity of the critical value.

Hartman and Lazarus (13) explored the pressure distribution on the axis of jets at reservoir pressures up to 7 kg/cm^2 using a pitot tube. Axial pressure curves were obtained in jets exhibiting both the simple X and the more complex Y shock interaction observed by Mach. The pitot measurements were in agreement with measurements of the Mach number using probes, in the case of the simple X interaction. These measurements constitute the best quantitative data we have found so far for supersonic jets, but are far from complete as only the axial region is explored. The schlieren photos made by Hartman and Lazarus are valuable for qualitative examination.

Prandtl (14) was the first to describe the formation of a free jet by determining what shape and direction a very weak shock wave, or sound wave ("Mach line") would assume at various parts of the jet. He showed that the wedge-shaped expansion region which arises from the orifice edge as the gas stream turns outward into the atmosphere (see especially his figures 7 and 9) is reflected from the opposite free boundary of the jet with a change of phase, and proceeds onward as a compression region, is again reflected as an expansion region, and so on, producing the periodic structure of the jet. Prandtl does not discuss the shock formation observed by Mach in jets.

II. OPTICAL METHODS OF STUDYING GAS FLOW

Optical methods of observation have an advantage over all other types as the gas flow is not disturbed by the light beam. Three experimental techniques are available, namely, shadow, schlieren, and interference photography. The production of shadows by the gas stream in a parallel light beam is a very simple method, and provides a wealth of information. This method is sensitive to the rate of change of gas density gradient, and is widely used in ballistics as it reveals the positions of shock waves and other discontinuities of density, and admits of a limited quantitative evaluation. Toepler's schlieren technique is also widely used, principally for qualitative examinations, where it is more sensitive than shadowgraphy at the expense of more complicated equipment (15). This method is responsive to the density gradient, and except perhaps for the Ronche variation, is not suited for quantitative studies. Shadow or schlieren photographs are valuable supplements to interferometric measurements.

The measurement of interference fringe displacement produced by an interferometer gives an accurate quantitative value for the density itself. The most suitable interferometer for studies in gas dynamics is the instrument developed by Zehnder and simultaneously by L. Mach for this purpose (16). Mach used this instrument for studies in ballistics and air jets (see reference 9). Reference 17 gives a bibliography

of all additional papers dealing with applications of interferometry to gas dynamics which have come to the writer's attention. Of particular interest is the article by Hansen (17-B), which describes the construction and simplified theory of a large Mach interferometer constructed for Russia by the Zeiss works in 1930, and that of Schardin (17-F), which gives more completely the theory of the instrument, and a simple method of evaluating the results for cases of circular symmetry. An analytical discussion of the shadow, schlieren and interferometric methods, including methods of evaluation, is given by Weyl (18-B).

Optical methods are sensitive only to the density, whereas one usually needs to know the other variables of the gas stream, such as pressure, temperature, and velocity. These can only be calculated from the measured density at each point by following the gas along a streamline from some point where the variables of state are known to the point in question, with the aid of gas dynamical laws which apply at each step of the way. This may involve calculating or measuring the streamlines themselves. In cases where this cannot be done, one or more other variables in addition to the density must be measured to define the state of the gas, which implies using non-optical means such as static pressure sounds, pitot tubes, thermo-elements, or probes to supplement the interferometric results. Since in the air jet described in this paper all streamlines are equivalent, beginning under identical

conditions in the reservoir, the same equations for pressure, etc., apply to all, at least up to the place where the streamlines cross a shock front. Consequently, the pressure and other variables may be calculated with a knowledge only of the density at the point in question and the reservoir conditions. In this report the necessary gas-dynamical relations will be stated or developed when needed in the discussion.

III. DISCUSSION OF THE MACH INTERFEROMETER

1. Description of the interferometer and of associated optical apparatus.

Figure 1 is a schematic diagram of the interferometer and associated optical equipment. Light from the source S, made parallel by the lens L_1, is divided at the surface of the partially reflecting plane-parallel plate 1, the reflected beam A proceeding to the plane mirror 3 and the transmitted beam B to the plane mirror 2. The two beams are recombined at the surface of the partially reflecting plane-parallel plate 4, which is identical with 1. The two beams are coherent, and produce interference fringes, which are then focused on the screen P by the lens L_2.

Figure 2 shows the interferometer and its mounting. The base is a piece of channel steel, to which the supports of plates 1 and 4 are screwed permanently. Plates 2 and 3 are mounted on carriages, which are guided by attached ball bearings sliding in grooves, and are moved with the traversing screws T-2 and T-3 for changing the path length in the two beams of the instrument.

Each plate is held against blocks by light springs in a rectangular frame to avoid stresses on the glass. This frame is held by three strong springs against ball-bearing ends of three regulating screws which are threaded through the main support, and two of which terminate on the other end in knurled knobs for adjustment. A movement of screw V rotates the plate about a vertical axis passing through the tips of H and a fixed

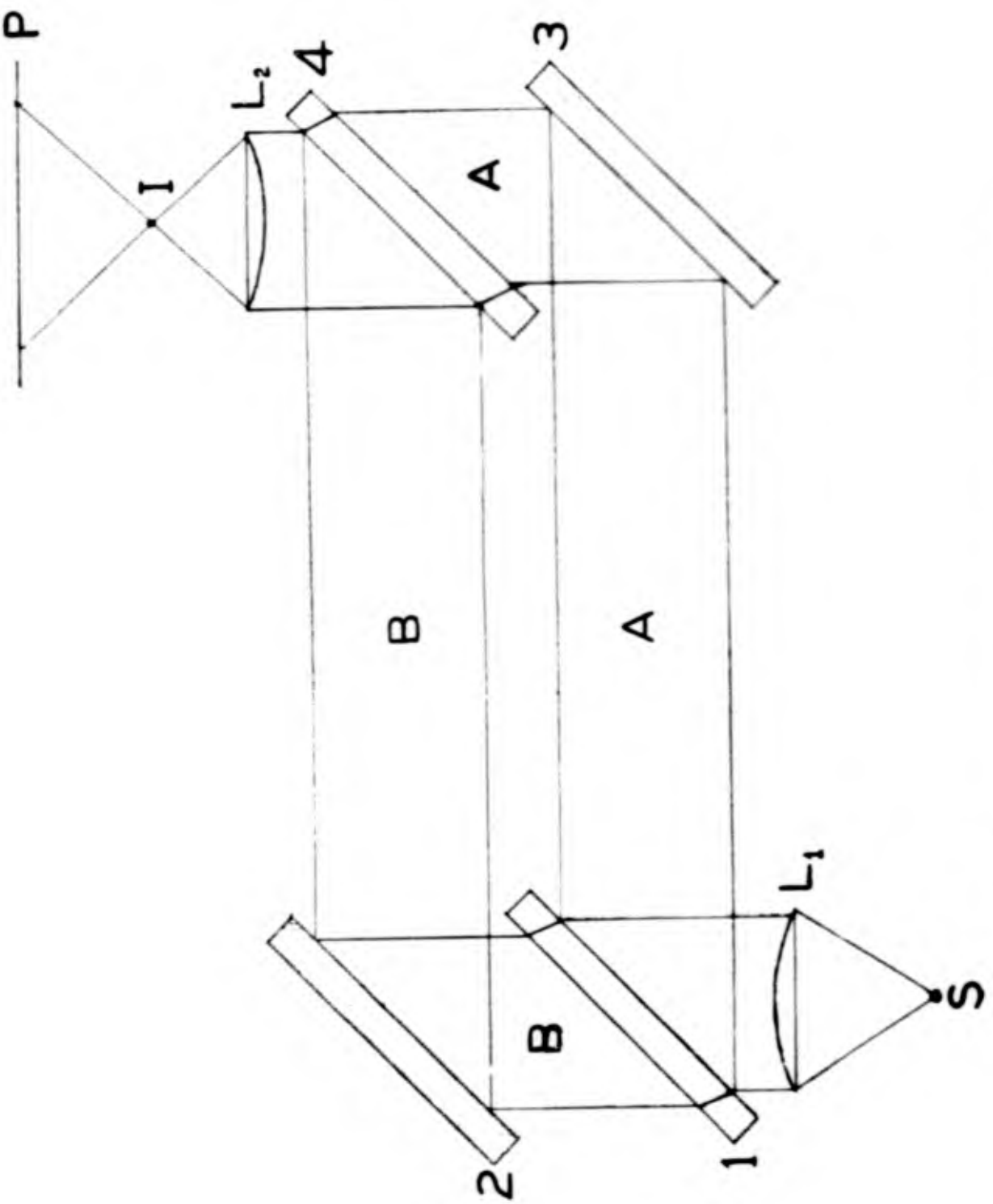

Fig. 1. Principle of the Mach interferometer.

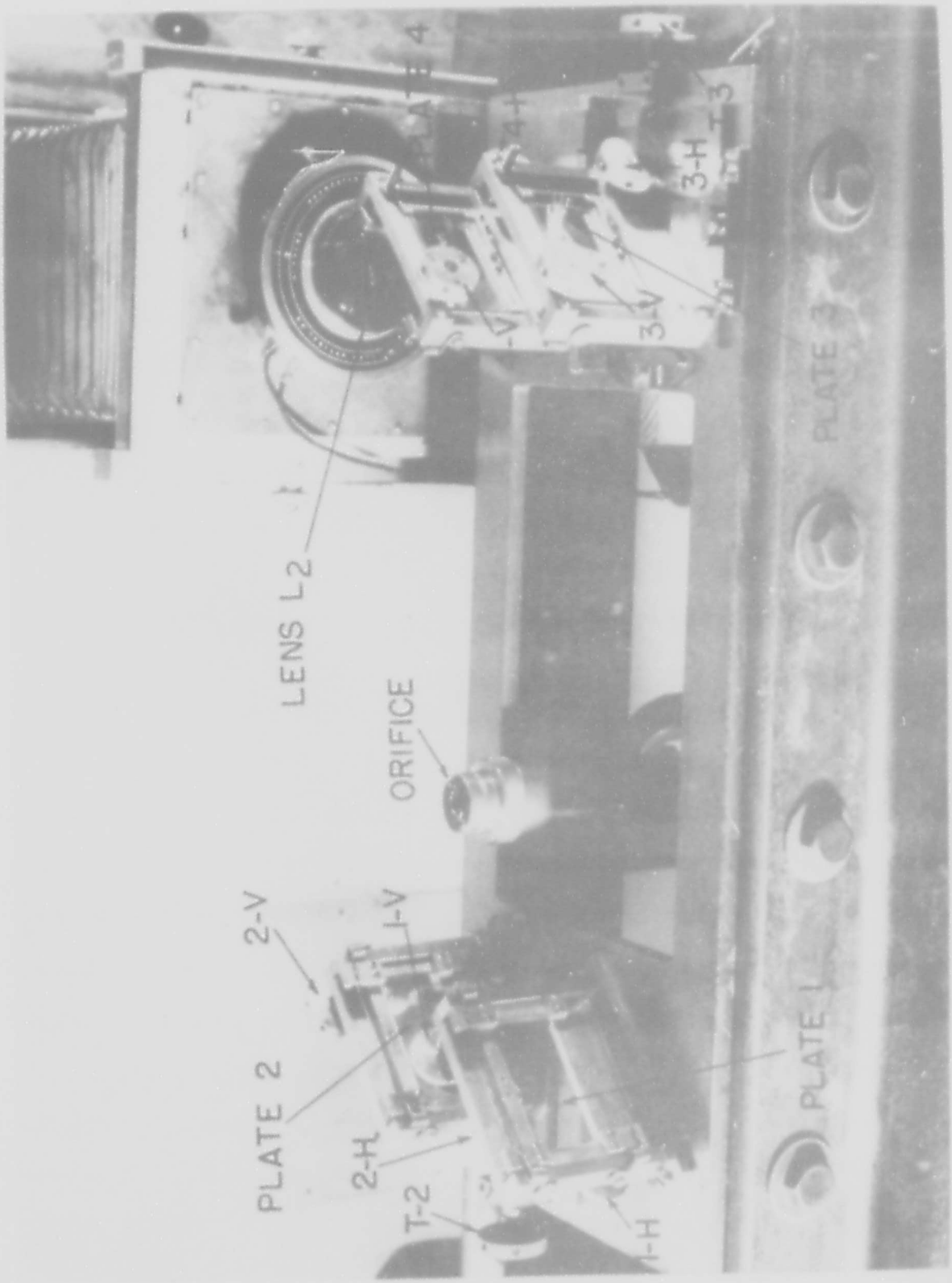

FIG. 2 VIEW OF INTERFEROMETER

screw. Similarly, an adjustment of H moves the plate about a horizontal axis through the tips of the fixed screw and V.

The means for adjusting the plates is not ideal, as the various motions are not independent, that is, movement of the plates about a horizontal or vertical axis also changes the path lengths in one or both beams of the interferometer. This is not a serious drawback, however, as compensating adjustments can always be made.

This interferometer was installed in a special laboratory at ground level on concrete foundations and insulated by rubber cushions against vibrations.

2. Theory of the instrument.

(a) Formation of the fringes. -- It is convenient to think of the instrument in terms of the two coherent images which may be observed at I (see Figure I) if light from a point source S is used, and if the plates are nearly parallel to one another. The light proceeds on from these images and produces interference fringes in much the same way as in Young's famous experiment, and the fringes are found to be sharp at any position of the screen P. If the images lie on a horizontal line, the fringes will be vertical, and vice versa. Narrower fringes are produced by displacing the coherent images farther from one another by rotation of one of the plates. If the lens L_2 is removed, fringes will still be observed, but the coherent sources are now virtual, and are located at infinity. (see Schardin, reference (17-F) Fig. 2, p. 398). Actually the fringes are hyperbolic, but the deviation from straight, evenly

spaced parallel lines is negligible over the usual working section.

When white light is used, the interference fringes disappear when the path difference exceeds a few wavelengths.

If instead of the point source at S, an extended source of light is used, fringes may still be observed, but now they will be sharp only in a particular plane. The reason for this is shown by Schardin (17-F). It must be considered that instead of two coherent point images at I we now have many pairs of coherent points, covering the whole extent of the images of S at I. It is requisite that the planes of symmetry of these point pairs intersect on a line (vertical line for vertical fringes, and horizontal line for horizontal fringes) if good fringes are to be observed. This line will then lie in the plane in which the fringes appear sharp. This condition may be brought about by a proper adjustment of the plates. For a horizontal linear extended source as treated by Schardin, and beginning with all plates parallel to one another, two plates must be rotated about a vertical axis to locate the fringes in a given plane. For a point source fringes will appear everywhere if only one plate is rotated. Although Schardin specifies the motion only of plates 1 and 4, actually the motion of any two plates will suffice for this adjustment.

If the fringes lie in a plane anywhere on the incident side of plate 4, they are virtual, and can be seen only by using the lens L_2 to focus them on P. Real fringes may be seen directly on P without a lens, however, if they are formed in a plane farther from S than plate 4.

The formation of second or higher series of interference fringes by multiple reflection at the surface of the plates is prevented by coating plates 1 and 4 with a partially reflecting aluminum layer.

The complete theory of the formation of interference fringes from a large extended source by the Mach interferometer has not been given so far. It has been repeatedly observed that if the interferometer is properly adjusted, the fringes may still be seen if the light source be varied from a distant point to a large diffuse area just before plate 1. We have found, however, that, as the fringe spacing is decreased, more nearly parallel light must be used to preserve the visibility or the fringes in the field of view.

(b) Formation of interferograms. -- (i) Production of fringe shifts. If a density disturbance is present in one beam of the interferometer, the fringes will be distorted in a definite manner from their normally straight and uniformly spaced condition. For an air jet in which the density of the air is a function only of the radius r and the distance from the orifice, z, the shift S(y) of a fringe maximum on the screen from its undisplaced position in units of the separation of two adjacent maxima in the undisplaced pattern is given by

$$S(y) = \frac{1}{\lambda} \int_{-d(y)}^{d(y)} [n(r) - n_o] \, dx \qquad (1)$$

In this equation λ is the wavelength of the light used, $n(r)$ and n_o the refractive indices corresponding to this

wavelength in the jet and for the ambient air, respectively, x the distance along a light beam which penetrates the jet at a distance y from the jet axis, and $+ d(y)$ and $-d(y)$ the values of x at the jet boundary. $S(y)$ is also a function of z, which is a constant for a given cross section. The refractive index n is related to the air density ρ by the Gladstone-Dale formula,

$$n - 1 = K\rho \quad , \tag{2}$$

where K is a constant.

Equation (1) is valid if the light beam in the arm of the interferometer is strictly parallel. The integral represents the increase in optical path length through the jet compared with the undisturbed beam of the interferometer, and division by λ gives the retardation in wavelengths of points in the wave front after it passes the jet. The reason that this may be equated to a sidewise shift of the fringes at various points on P may be understood by reference to Fig. 3. I and I' are two coherent images of a point source S, formed by the lens L_2. Bright fringes are normally produced on P at the positions 1, 2, 3, and so forth, where the lines along which the wave fronts from I and I' reinforce each other intersect P. If the wave fronts are retarded, as shown by the dotted lines, the line of reinforcement is shifted to I'. Since successive orders of interference produce fringes that are evenly spaced on P, it follows that the displacement of I' from I is proportional to the fractional retardation in wavelengths of the dotted wave front. It is evident that the

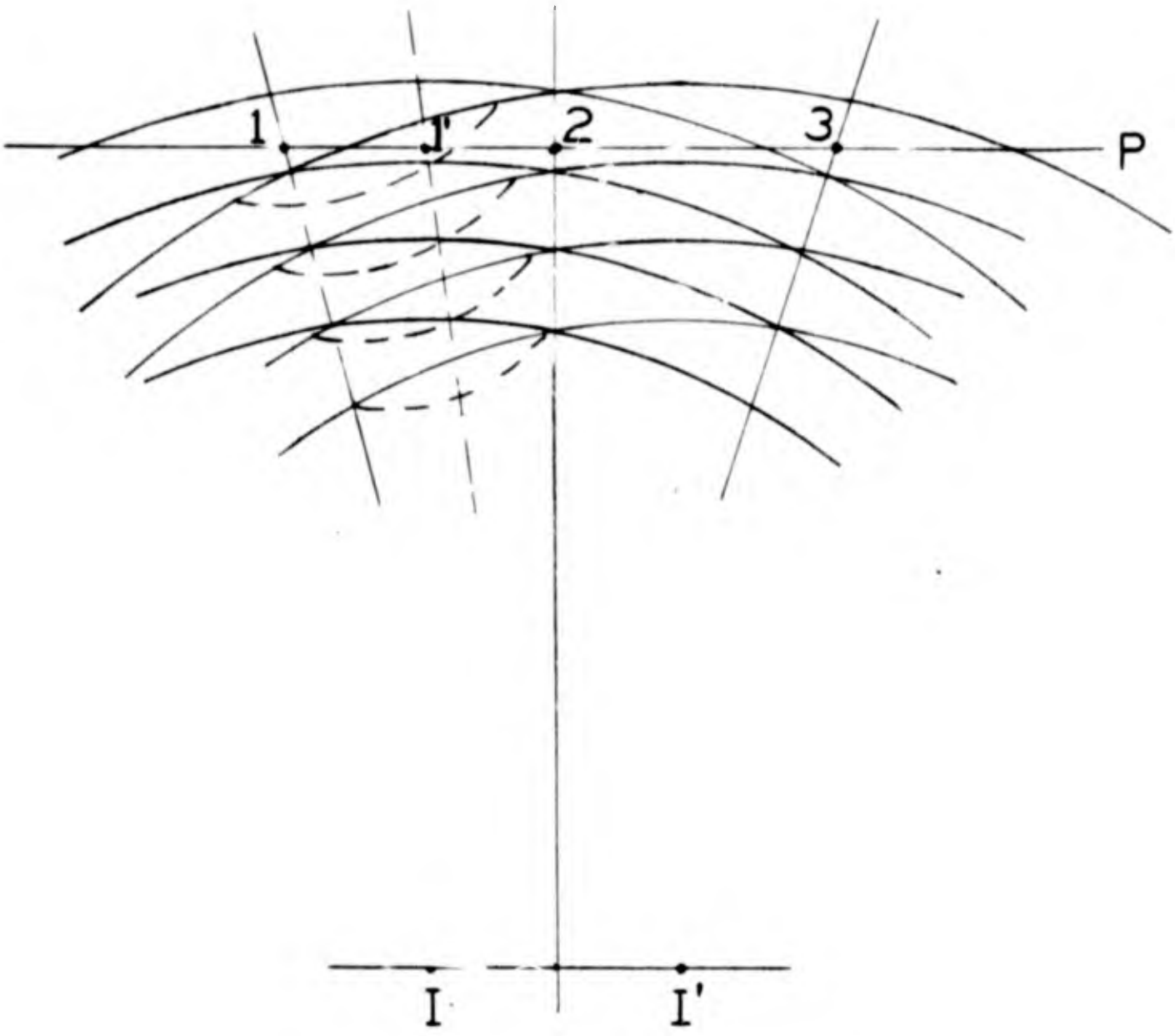

Fig. 3. Production of an interferogram.

intensity distribution is also distorted from that of the undisplaced fringes. The direction of fringe shift can be reversed by changing the density disturbance to the opposite beam of the interferometer, giving a complementary interferogram. The same result can be obtained merely by adjusting the interferometer plates so that the images I and I' (Fig. 3) are interchanged. This picture is of course simplified somewhat, as actually an irregular retardation of the wave front implies a change in the direction of the rays so that some would not pass precisely through I and I' on their way to the plate. The actual angle through which the light ray is refracted in passing through the jet may be determined from the fringe spacing, for if the undisplaced fringe spacing d_o represents an angle α_o between the light beams in the two arms of the interferometer, then a spacing d represents an angle α, approximately, according to the relation

$$\frac{\alpha}{\alpha_o} = \frac{d_o}{d}$$

(ii) Fringe width and orientation. The fringe shift S, expressed in units of the undisplaced fringe spacing at a point on P, is independent of the spacing or orientation of the undisplaced fringes, but the appearance of the pattern varies greatly if wider or narrower fringes are used.

Figures 4(a), (b) and (c) show three interferograms of an air jet from a 10-mm circular orifice at 60-lb/in^2 overpressure in the tank, made by focusing the fringes parallel

(a) Fringes parallel to axis

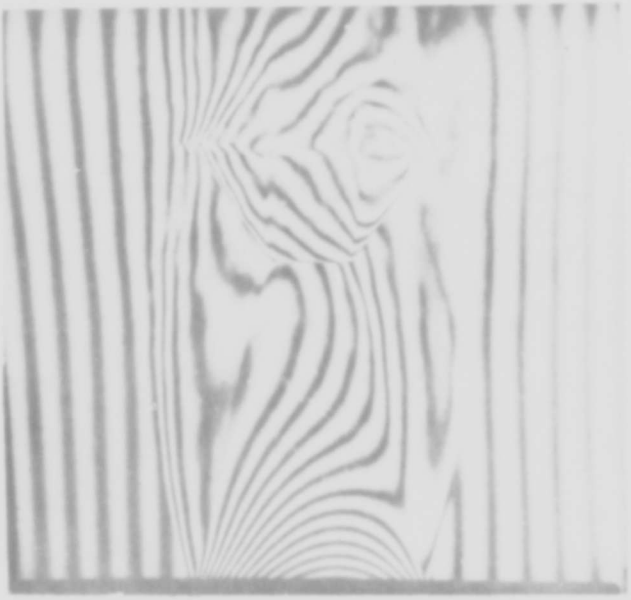

(b) Fringes parallel to axis

(c) Fringes parallel to axis

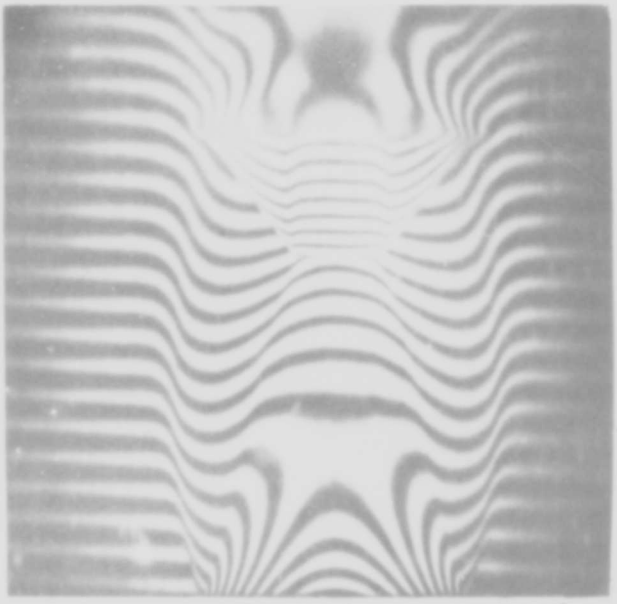

(d) Fringes normal to axis

Fig. 4. Effect of fringe width and orientation.

to the jet axis. The fringe width increases from (a) to (c). These interferograms were made by producing the fringes virtually in the plane of the jet axis, and focusing the fringes and orifice together on a photographic plate at P. The illumination was produced by the light source which is described in Part III-5. A detailed analysis of this jet is given in Part VI. The reason for the asymmetrical appearance is also explained there.

The jet boundaries and shock fronts in Figs. 4(a), (b), and (c) have the same location, but in (b), and especially (c) "islands" are formed at several points. The explanation of the formation of these islands is simple, and is illustrated in Fig. 5. The curves in Fig. 5 (a) are the fringe shifts at points along three cross sections through a simple assumed interferogram. In Figs. 5(b), (c), and (d) these fringe shifts are graphically carried out in narrow, medium, and wide fringes. Wide fringes are moved farther from their original position than narrow fringes, so the same fringe can cover regions of considerably different optical retardation, producing an island. A sufficient increase of the density gradient in the jet would produce islands even with narrow fringes.

We have found the following rules useful:

(1) Orient the fringes parallel to the axis of symmetry of the density pattern under investigation.

(2) Make the fringes as narrow as possible.

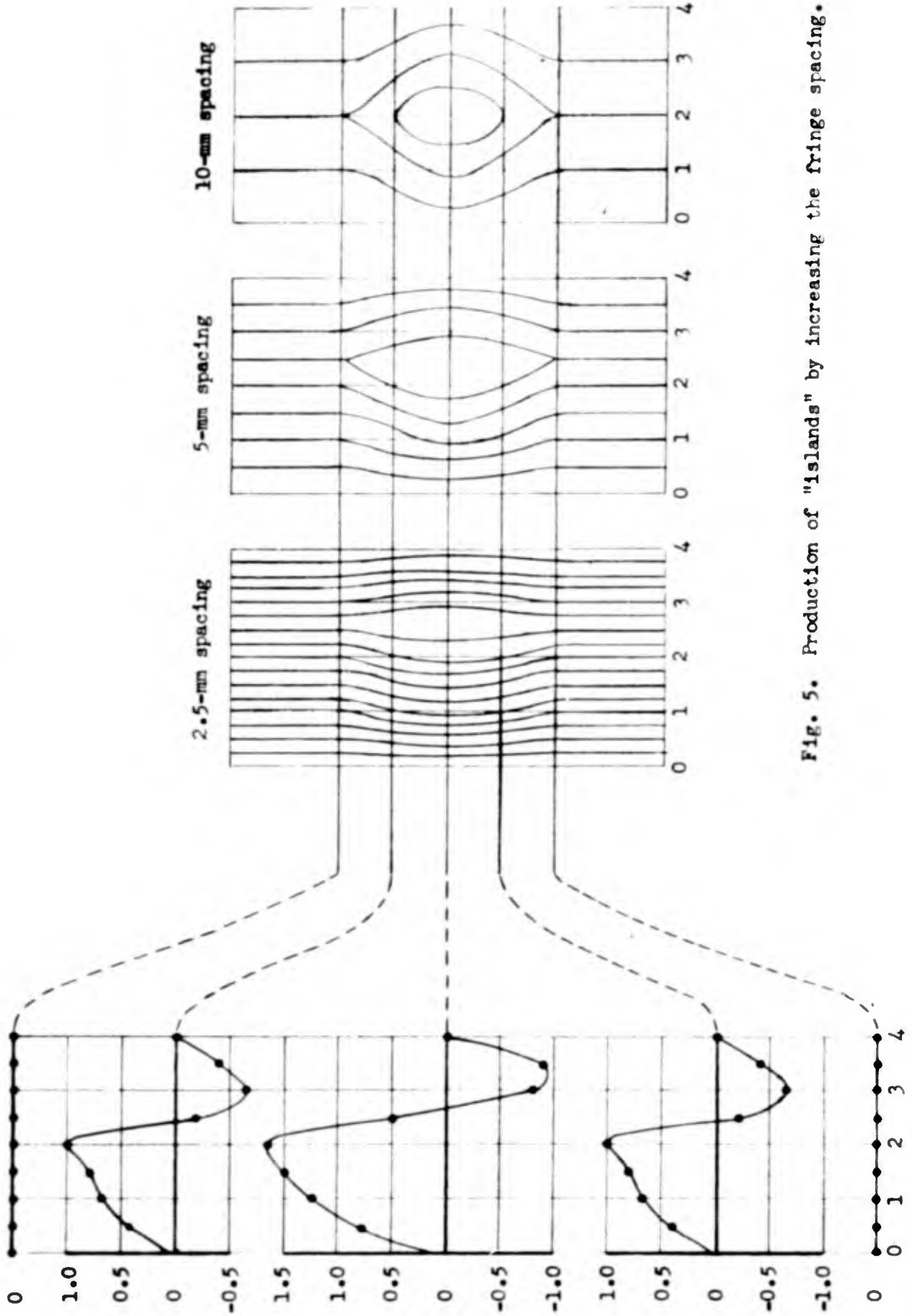

Fig. 5. Production of "islands" by increasing the fringe spacing.

BLANK PAGE

If the density is to be evaluated in a given cross section normal to the axis, measurements then proceed across the fringes if rule (1) is followed. Fringe-shift values are obtained directly from the measured fringe positions, and each measured cross section is independent of others.

On the other hand, if the fringes run across the pattern, normal to the axis of symmetry, measurements must be made on each fringe along a line parallel to the axis. The fringe shifts in a cross section must then be obtained by a troublesome extrapolation. Single cross sections cannot be obtained in this way without much extra labor. This orientation of fringes has merit only if, when oriented as in rule (1), too few fringes are available to cover the field.

Figure 4(d) shows an interferogram of the same jet as in Figs. 4(a), (b), and (c), but with horizontal instead of vertical fringes. The pattern is now symmetrical, but the fringe shift at each point is still the same as in Figs.4(a), (b) and (c).

Since each fringe maximum and minimum produces a measured point, narrow fringes produce more points in a given region; hence rule (2). This is especially important across shock fronts, where fringe shifts are large and points are separated more. Narrow fringes also tend to eliminate islands, as shown in Fig. 5, and thus eliminate uncertainty in numbering the fringes.

Further remarks on use of fringes are given in Part V, Sec. 1.

(iii) Use of nonparallel light. If nonparallel light is used to produce the interference fringes, Eq. (1) is no longer strictly valid. The situation in this case is shown in Fig. 6. One beam only of the interferometer is considered, and for simplicity the interferometer plates have been omitted. The jet and fringes are imaged by the lens at P. If parallel light were used, only ray 2 would contribute to the image of point A in the jet at A'. But with a broad light source, a bundle of rays limited by 1 and 3 arrives at A', and each ray experiences a different retardation in passing through the jet. (If the jet were absent, the optical length of all rays from A to A' would be equal.) We would therefore expect a washing out of the fringes at P. The effect should be especially pronounced if the density in the jet varies rapidly with the radius, as for example across a shock, which is shown in Fig. 6 by the light and shaded areas in the jet.

Figures 7(a) and (b) show two interferograms of the same jet made (a) with parallel light from a short fine slit and collimating lens, and (b), with diffuse light from a ground glass just before plate 1 (see Fig. 1). These two interferograms, as well as other such pairs made with much narrower fringes, yield identical fringe-shift values, within experimental errors, and the only observable difference is some loss of contrast as in Fig. 7(b). (Blurring of shocks is due to slow shutter speed.) We conclude from this that the aperture of the optical system, even with the diffuse

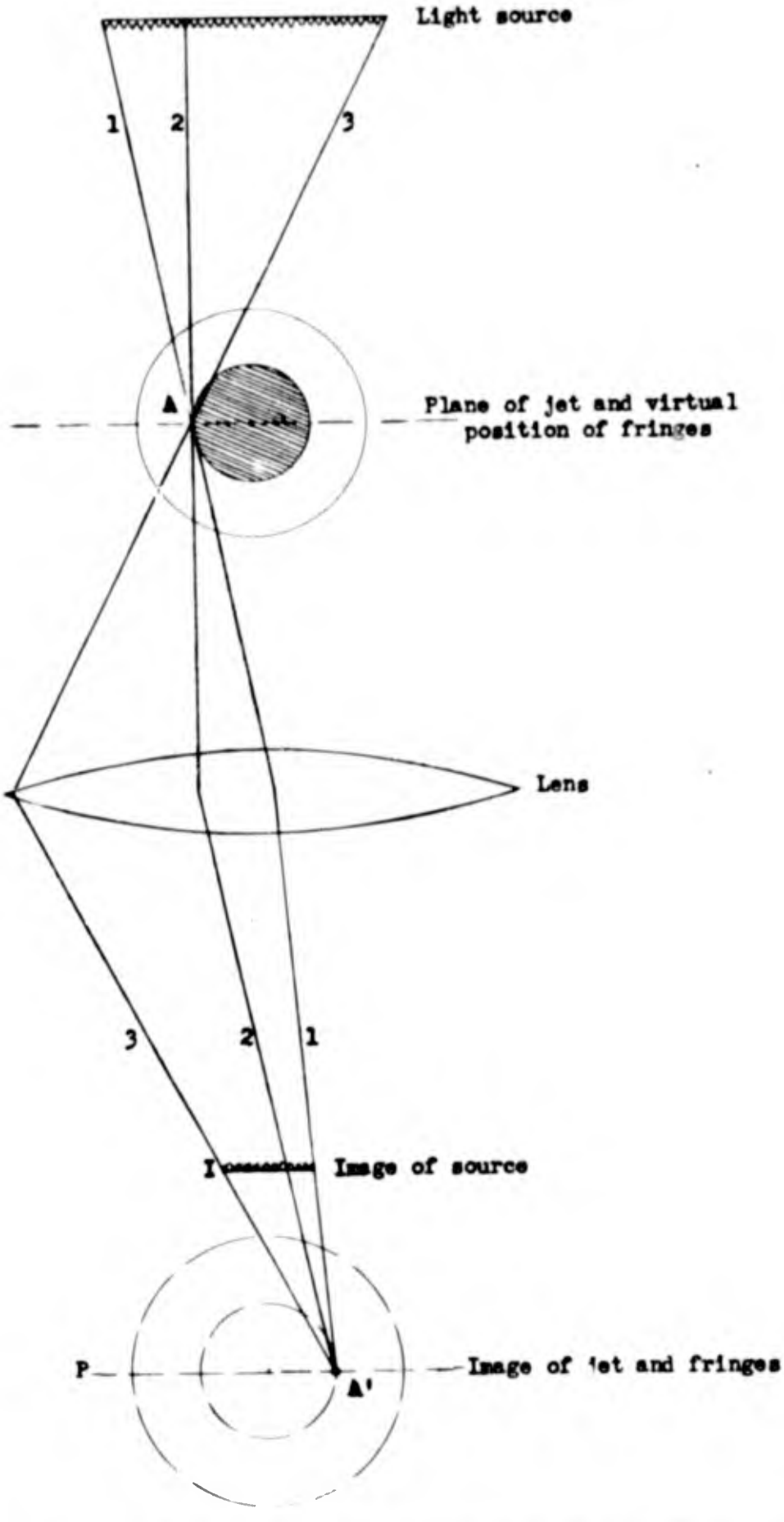

Fig. 6. Production of an interferogram by nonparallel light.

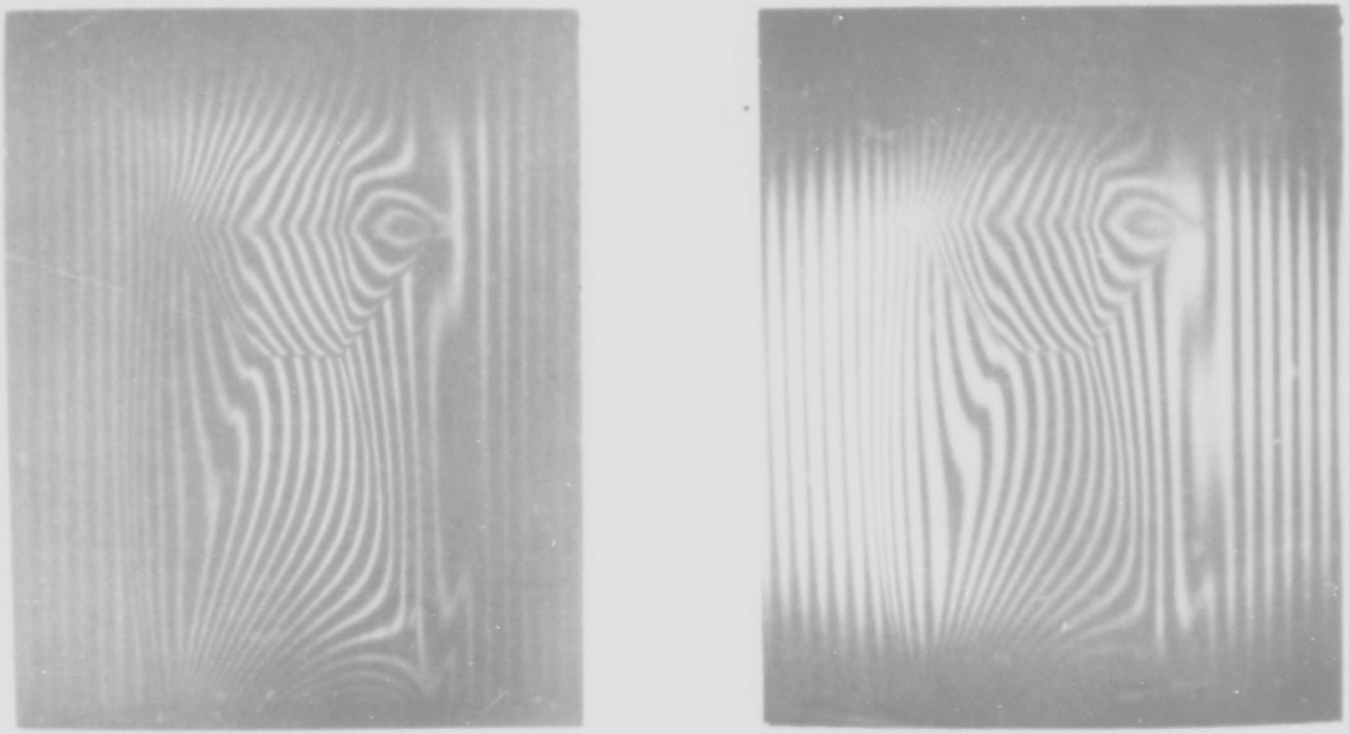

A
Parallel Light

B
Diffuse Light

Fig. 7. Interferograms produced by parallel and by diffuse light.

BLANK PAGE

source, is small enough to limit the divergence of rays passing through the jet to a satisfactorily small value.

(iv) Refraction effects in the density pattern. Refraction of the interferometer beam in passing through the air jet, due to the lens action of the regions of different density, cannot be avoided. If parallel light is passed through the jet, and a screen is placed beyond it, a shadowgram of the jet will be formed, with regions of large density gradients (such as shock fronts) revealed by adjacent dark and bright bands, the bright band being toward the region of greatest density. The theory of formation of shadowgrams has been studied by Keenan, (18-A) and Weyl (18-b)

In Fig. 8 parallel light traveling in one beam of the interferometer (which is omitted for simplicity) passes the jet and falls on the lens L. If the lens is focused not on the jet itself but very slightly before or behind the plane of the jet, a shadowgram will be formed on P. Figure 9 shows this phenomenon in the same air jet used for obtaining Figs. 4 and 7. The narrow band of white-light fringes was formed by the total light of a spark, made parallel by a collimating lens. In Fig. 9 (a) the lens was focused in a plane traversed by the light beam just before entering the jet, in Fig. 9(b) on the exact jet center, and in Fig. 9(c) on a plane crossed by the beam after passing the jet. The relative positions of the light and dark bands at the shock is reversed in Figs. 9(a) and 9(c). The shadows disappear

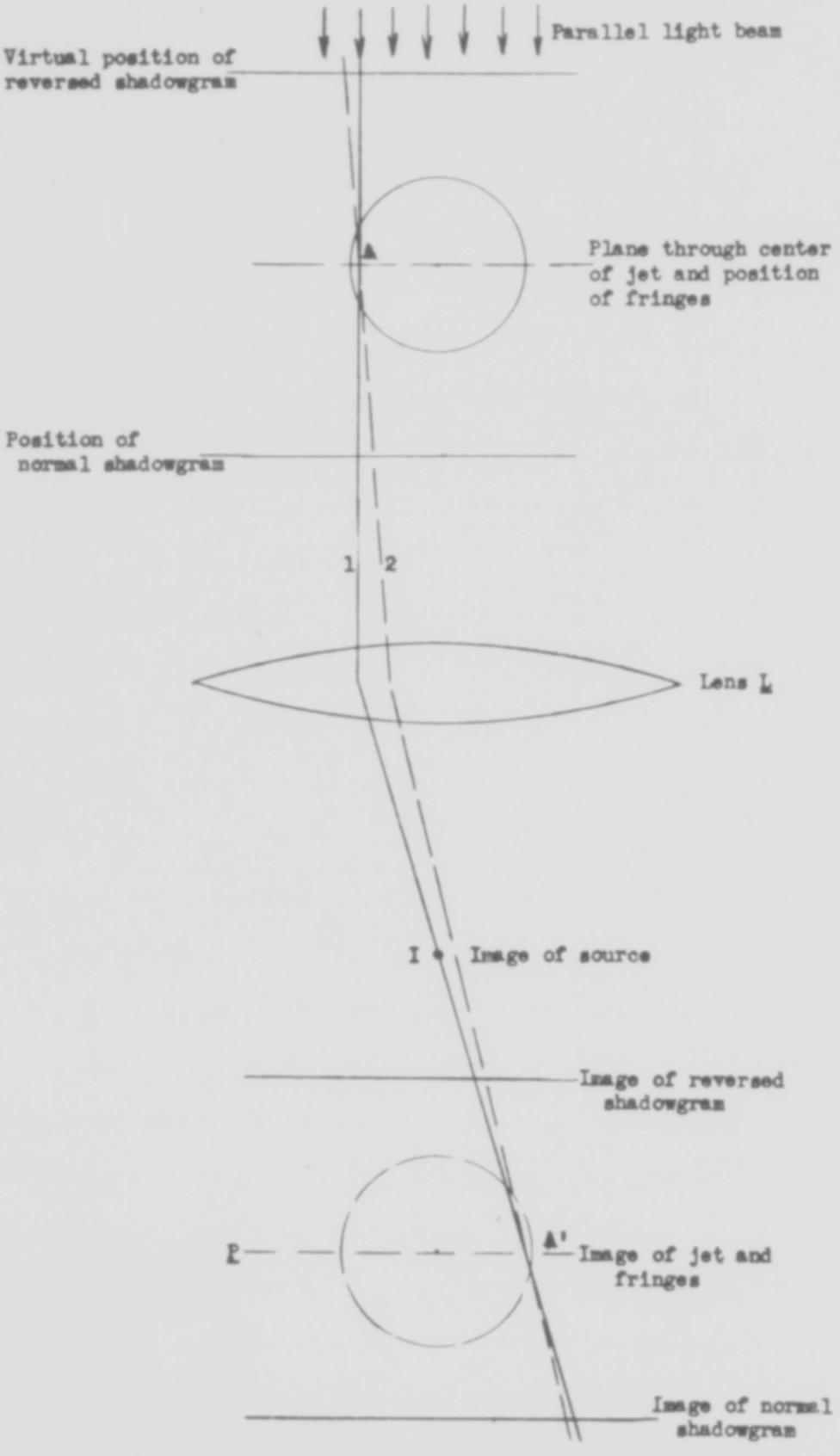

Fig. 8. Refraction effects in the production of an interferogram.

BLANK PAGE

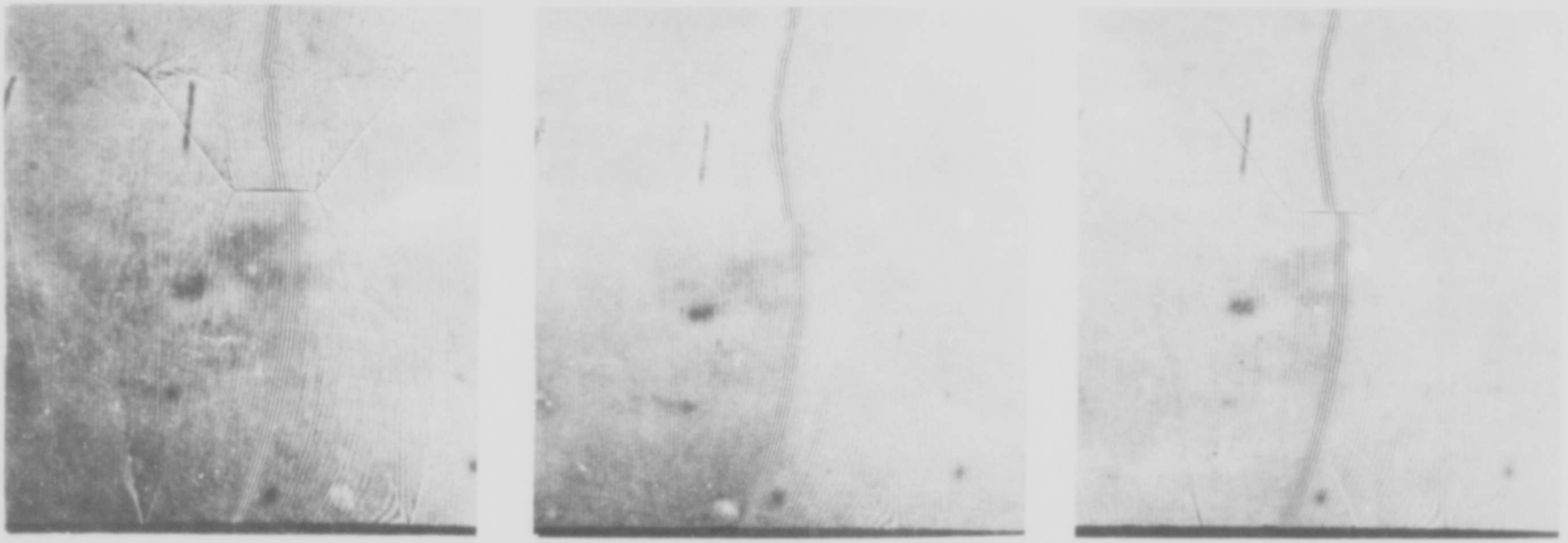

(a)

Lens focused in a plane traversed by the light beam before entering jet.

(b)

Lens focused on the exact jet center.

(c)

Lens focused on a plane traversed by the beam after crossing the jet.

Fig. 9. Sample interferograms showing the effects of refraction.

in Fig. 9(b) at the jet center in the case of the oblique shock. A shadow persists from the normal shock, probably because of its finite extension along the path of the light ray.

Returning again to Fig. 8, we see that without refraction ray 1 is undeviated by the jet, and proceeds from A to the image point A'. Actually, however, the ray is deviated, and follows the dotted path 2. The angle of refraction can be calculated from the shadowgraph theory (see reference(18)). If the lens is carefully focused, ray 2 will also arrive at A', and no shadows will be seen on P.

Now Fermat's principle tells us that for a perfect lens, the optical lengths of all rays from a point in the object to a point in the image are equal. Provided rays 1 and 2 are not separated very much on the lens surface, this principle still holds in practice for lenses of good quality. Furthermore, if we ignore any path differences between 1 and 2 while the rays are in the jet, we have the important result that for a good lens, carefully focused on the jet, no disturbances in the interferogram will result from refraction of light in the jet.

We have calculated the fringe-shift error arising from the path difference of rays 1 and 2 while in the jet, including the fact that 1 and 2 do not appear to come from the same point, and find it to be negligible (less than 0.01 fringe-shift units for the 10-S-60 jet described in Part VI. In the case of refraction by the z - gradient in

continuous regions of the jet, the effect is also negligible.

We have not devised a good experiment to test this result, but it is observed that under proper adjustment, fringes at shock boundaries are very sharp (see Fig. 15, for example). If the focus is not on the jet center, fringes in this region are blurred, even if parallel light is used.

In interferometers such as the Michelson type a given ray traverses the density pattern a second time after reflection from a mirror. Owing to refraction in the jet, the two paths through the jet are not necessarily the same, thus leading to serious complications in the interpretation of the results. Furthermore the Michelson fringes cannot be focused at will in an arbitrary plane.

3. Technique of adjusting the instrument. (See Hansen, reference 17-B)

The best way of adjusting the four plates is to place them on the corners of a square, and coat the mirrors 2 and 3 (see Fig. 1) for about 98% reflection. By the use of multiple reflections these two mirrors may be made precisely parallel. The two half-reflecting plates 1 and 4 may then be adjusted parallel to the mirrors by using two sets of cross hairs at two positions between L_1 and plate 1, and bringing the double images into coincidence.

In our case the plates were not arranged on a square, so that other less exact methods had to be used.

4. Photographic apparatus.

A 21-cm F/4.5 Zeiss Tessar lens of 5-cm diameter mounted in a 4 × 5-in. view camera with double-extension bellows has been used. A magnification of the jet and fringes on the photographic plate to twice actual size is generally used. Smaller images would increase the photographic density but also the ratio of grain size to fringe width, thereby decreasing the accuracy of measurement. Although in the case of circular jets the lens may be focused sharply on the jet center, if the pattern under investigation is two-dimensional, with a finite extension along the light path, the focal length of the camera lens must be long enough so that the near and far ends of the pattern are in focus simultaneously, within a satisfactory limit of distortion.

Eastman 103-G (fast) or III-G (slower, more contrast, and finer grained) spectroscopic plates have been used throughout our work. These plates have a maximum sensitivity in the green, suitable for the mercury line 5461Å. According to curves furnished by the manufacturer, a limited amount of photographic density could be gained by using violet light and correspondingly sensitized plates.

5. Light sources for interferometry.

The ideal light source for interferometry needs to be monochromatic, as well as intense and of short duration. We have found that even for jets where the phenomenon is

"stationary," an exposure of less than 100 μ sec. is desirable. Longer exposure times often show two or more traces of the shock boundary owing to sudden small shifts of its position.

The wavelength increment $\Delta\lambda$ that can be tolerated depends on the number of fringes required. For n satisfactory fringes,

$$\Delta\lambda = \frac{\lambda}{3n} \qquad (3)$$

is a safe estimate. We have tried the following light sources:

(i) Cenco laboratory mercury arc with small diaphragm; 8-cm diameter 70-cm focal-length telescope objective; Corning filters Nos. 3484 and 5120 for isolating the green line 5461 $\mathring{A}$ (some red also included); camera shutter at 1/100 sec. This source gives good fringes but in general is not fast enough.

(ii) General Electric type AH-6 1000 watt water-cooled mercury capillary arc; lens and filter same as in (i); 300-μsec mechanical shutter, consisting of one fast and one slow motor-driven disk, each containing a suitable slit giving a flash every 3 sec; arc operated from a d-c generator at 800 volts instead of 1000 in order to lower pressure and improve sharpness of spectral lines. This source is superior to that in (i) but not fast enough for general use. (See Fig. 15 of this report for an interferogram made with it).

(iii) General Electric type AH-6 capillary arc flashed with a condenser discharge; voltages from 2000 to

8000 and capacities from 0.25 to 4 μf; filters for the mercury green line as in (i); about 25 good fringes can be obtained with this arrangement. The time duration is between 10 and 100 μsec, fast enough in general for jet interferometry. Only the very turbulent region at the boundary is not stopped by this flash. Figures 19 and 20 are shadowgrams taken with the full light of this mercury flash.

(iv) General Electric type AH-6 capillary arc flashed with a condenser discharge as in (iii), and the light sent through a very large aperture (about F/2.5) prism monochromater. The 3-cm long exit slit was curved to fit the spectral lines from the prism. Under the best conditions, by compromising between slit width and exposure, 100 fringes have been obtained, with some sacrifice of fringe focus at a few spots in the field. A noticeable improvement in focus was obtained by limiting the long exit slit to 5 mm, but the necessary widening to secure exposure resulted in considerably fewer fringes.

(v) Spark of the Charter's type, with aluminum electrodes. The 1/2-mm hole through which the light emerges was substituted for the entrance slit of the large monochromater described in (iv). A yellow-green line, which gave the most exposure was selected. About 20 usable fringes could be obtained with this source. Narrowing the slits gave more fringes, but underexposed plates.

This type of spark is rapid enough for nearly every application. ($\approx$0.5 μsec. from rotating mirror measurements).

(vi) a very satisfactory light source for all purposes has proved to be an unconfined air spark between vertical magnesium electrodes, the light being sent through a large prism monochromator. With the aid of a photocell, the strongest spectral line may be selected (4481 A), which has an intensity about twice that of the underlying continuum. With this arrangement about 200 usable fringes can be produced, with illumination times of about 1 μsec., and a photographic image of about $1\frac{1}{2}$ x 2 inches. Because of the low intensity ratio between the spectral line and the continuum, filters alone over this spark would produce only a few fringes (10 - 20).

Light source (ii) was found suitable for interferograms of the 10-S-60 air jet studied in this report, as this jet is relatively "smooth". The spark source (vi) has been used for jets at 40, 80, and 100 lbs., which are more turbulent than the 60 lb. jet.

IV. AUXILIARY APPARATUS FOR STUDYING GAS JETS

1. General arrangement

The air jet for investigation was supplied from a $1\frac{1}{2}$ m^3 tank which was filled with dry air at pressures up to 120 lbs/in^2 fed from high-pressure gas cylinders pumped up on the Palmer Laboratory liquid air machine. The pressure and temperature could be accurately measured. The orifice and valve assembly is shown in Fig. 10. The valve when open forms a smooth-walled passage from the tank up and out of the orifice. The orifice is placed in one light beam of the interferometer (see figure 2), and is streamlined to produce a smooth flow by constricting the tube from the tank from 25 mm to 10 mm in the manner shown in Figure 10. The valve is either opened quickly by hand, and the light flashed by an automatic switch when the tank pressure drops to a predetermined value, or the valve is opened to synchronize with the rotating shutter.

2. Shadowgram apparatus

Shadowgrams of the air jets were made with the full light of the General Electric AH-6 arc flashed from a condenser discharge (see Part III, 5 - iii) focused on a pinhole 1 meter from the jet. Eastman 4 x 5-in type III-G spectroscopic plates were used, close to the jet (25 mm from the axis). Mach-number measurements were made by extending a steel needle, with a carefully ground conical point of 2° half-angle, into the stream, as nearly as possible along a flow direction, from above.

The Mach number is given by the equation

$$M = 1/\sin\alpha \qquad (4)$$

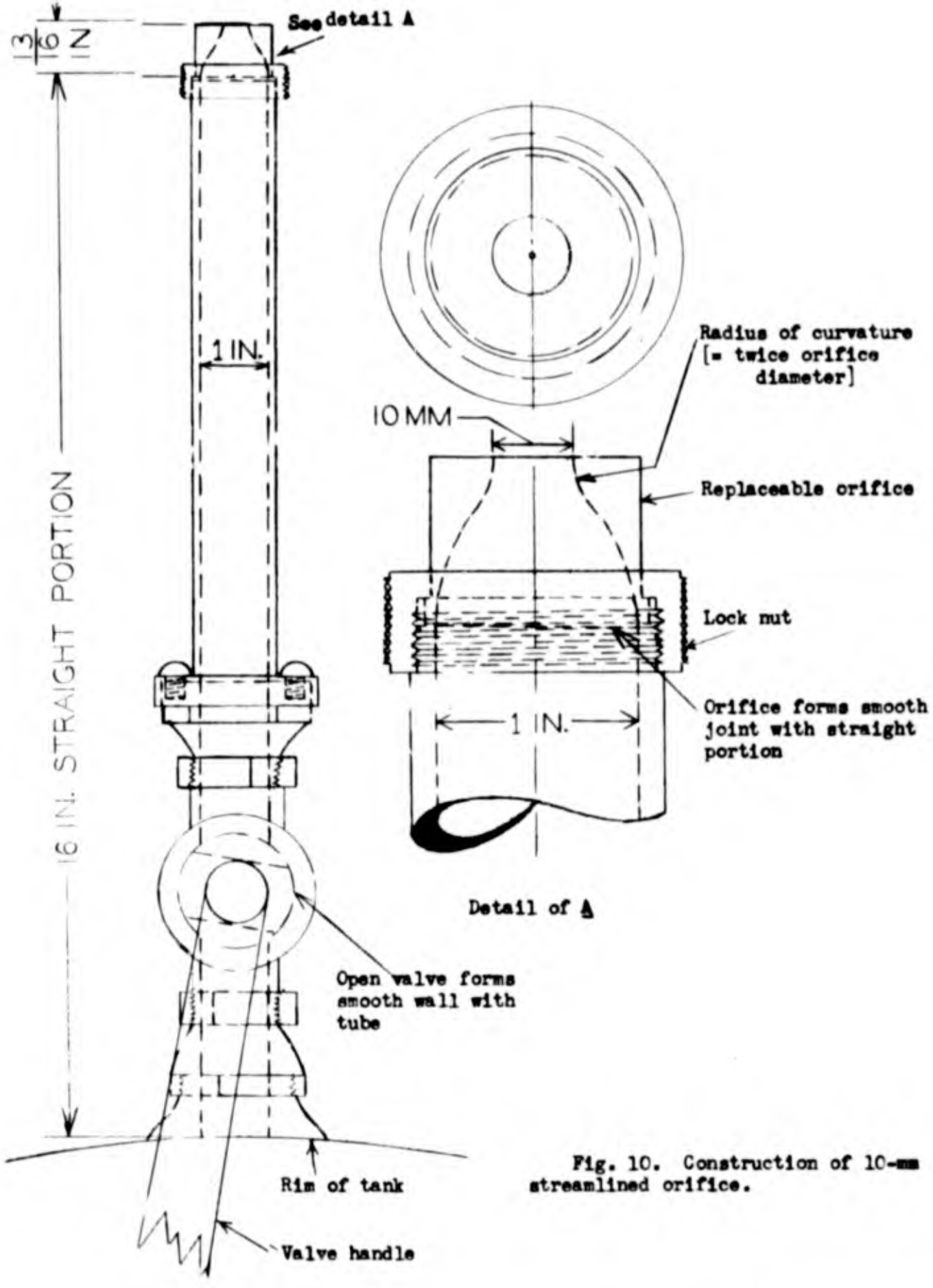

Fig. 10. Construction of 10-mm streamlined orifice.

where α is half the apex angle of the conical head wave, provided the head wave travels with local sound velocity. The correction given by Taylor and MacColl's theory (19) for the shock angle for this cone was only about 1 percent and was ignored.

BLANK PAGE

V. METHOD OF ANALYZING INTERFEROGRAMS

1. Measurement of plates

(a) Comparator method. -- The interferogram plate was mounted on a comparator table equipped with an accurate screw for measuring the y-coordinate (position in a cross section through the interferogram normal to the axis of symmetry), and having a less accurate gauge for obtaining the z-coordinate (distance of the cross section from the crifice mouth).

With the plate set at a definite z-value, and beginning with about the tenth fringe outside the region of the jet, the location of each maximum and minimum was recorded through the pattern to a similar point on the opposite side. Each cross section was measured twice, and the results were averaged. The procedure was varied to advantage by recording only maxima in slowly varying regions of the jet, and by recording maxima and minima three times in regions where shocks existed.

A plot of such readings, with fringe number as ordinate and position as abscissa, is shown in Fig. 12(A) for a special case (Fig. 4(B), cross section just above the normal shock).

(b) Automatic microphotometer method. -- The trace made by a Leeds and Northrup microphotometer with a Speedomax recorder 5/ of a portion of an interferogram is shown in Fig. 11. A region of sharp, strong fringes is shown in Fig. 11(a), and a region of broad, diffuse fringes is shown in Fig. 11(b).

5/ Through the kindness of R.C.A. Laboratories, Princeton, N.J.

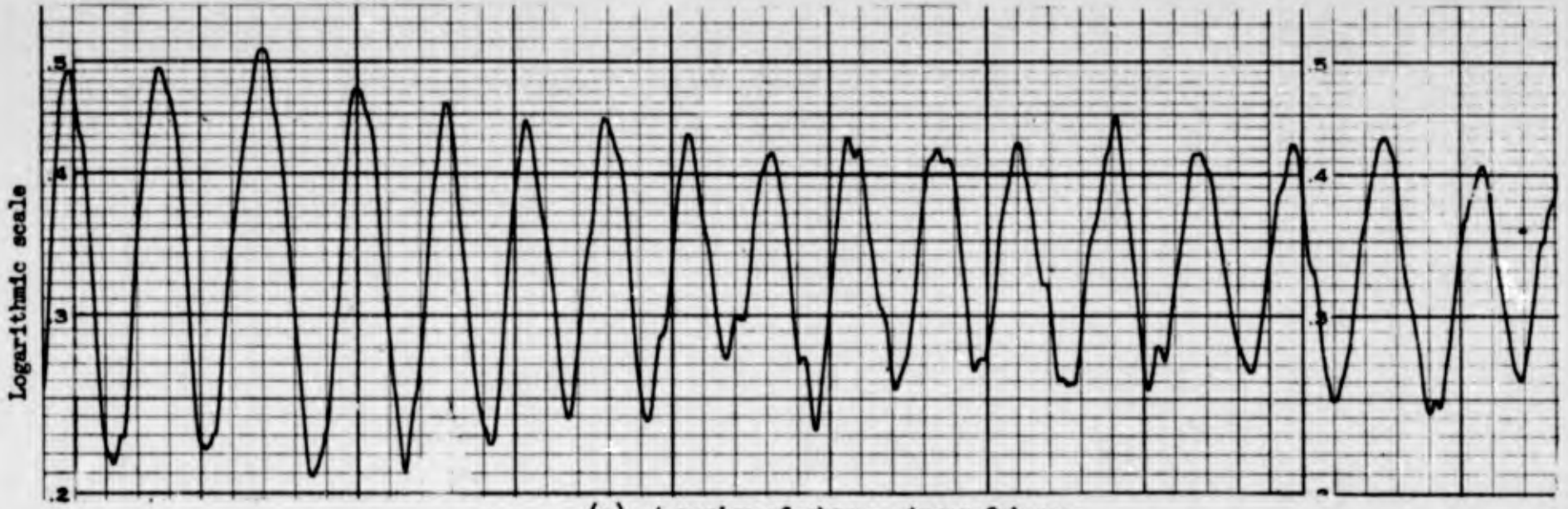

(a) A region of sharp, strong fringes.

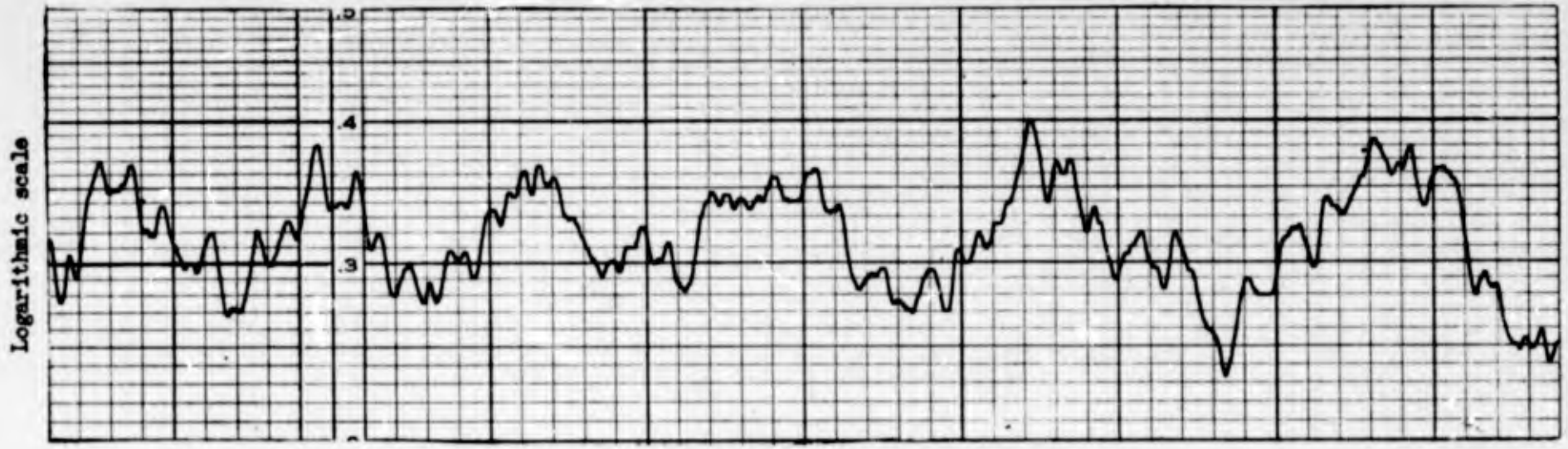

(b) A region of broad, diffuse fringes.

Fig. 11. Microphotometer traces of an interferogram.

BLANK PAGE

The positions of the fringe maxima and minima must be estimated from the trace, after which the results are treated in the same way as those obtained from the comparator.

Since the shifted fringes may be inclined to the vertical, a much shorter slit must be used for scanning the interferogram than is ordinarily used for a spectral line in order to confine the trace to a narrow cross section. This results in accentuated grain, as shown especially in Fig. 11(b).

The difficulty in locating the center of the fringe from the microphotometer trace can be appreciated from Fig. 11. We have found the comparator method to be more accurate, and usually quicker than the automatic recorder. In addition, the judgment of an observer using a comparator is needed to analyze a complex interferogram, particularly for numbering the fringes correctly, since the same fringe may be traversed more than once as the measurement proceeds across a given section.

In principle it is possible to obtain a very great number of measured points in a cross section by evaluating the intensity distribution through each fringe with the aid of the recording microphotometer. But the complications resulting from variations of fringe visibility and intensity over the field of view and the usual difficulties with the response of photographic emulsions, would make this procedure very laborious. We believe that it is more advantageous to increase the number of measured points by decreasing the fringe spacing.

2. Calculation and plotting of fringe shifts

The fringe shift, S(y), at a point (y, z) in the interferogram is given by the difference between the ordinates, N'-N (Fig. 12), of the observed curve of fringe location in a given cross section (z = constant), and the undisturbed curve (the straight dashed line) which exists without the air jet or other density pattern. It will be seen that this is equal to the movement of a fringe found at the point Y from its undisturbed position, expressed in units of the fringe spacing in the undisturbed pattern. The S(y) values were obtained from the data by using the equation

$$S(y) = \mp N \pm \left\{ y\left(\frac{N_1 - N_0}{y_1 - y_0}\right) + \left[N_0 - y_0\left(\frac{N_1 - N_0}{y_1 - y_0}\right)\right]\right\} \qquad (5)$$

or

$$S(y) = \mp N \pm (Ay + B)$$

A and B are constants for a given cross section.

$$A = \frac{N_1 - N_0}{y_1 - y_0}$$

$$B = N_0 - y_0\left(\frac{N_1 - N_0}{y_1 - y_0}\right)$$

N_1 and N_0 are two fringes in the undisturbed region close to the boundary of the disturbance, y_1 and y_0 being their correct positions in the cross section at z, determined as accurately as possible by measuring N_1 and N_0 many times, by averaging over adjacent undisturbed fringes on either side of N_1 and N_0

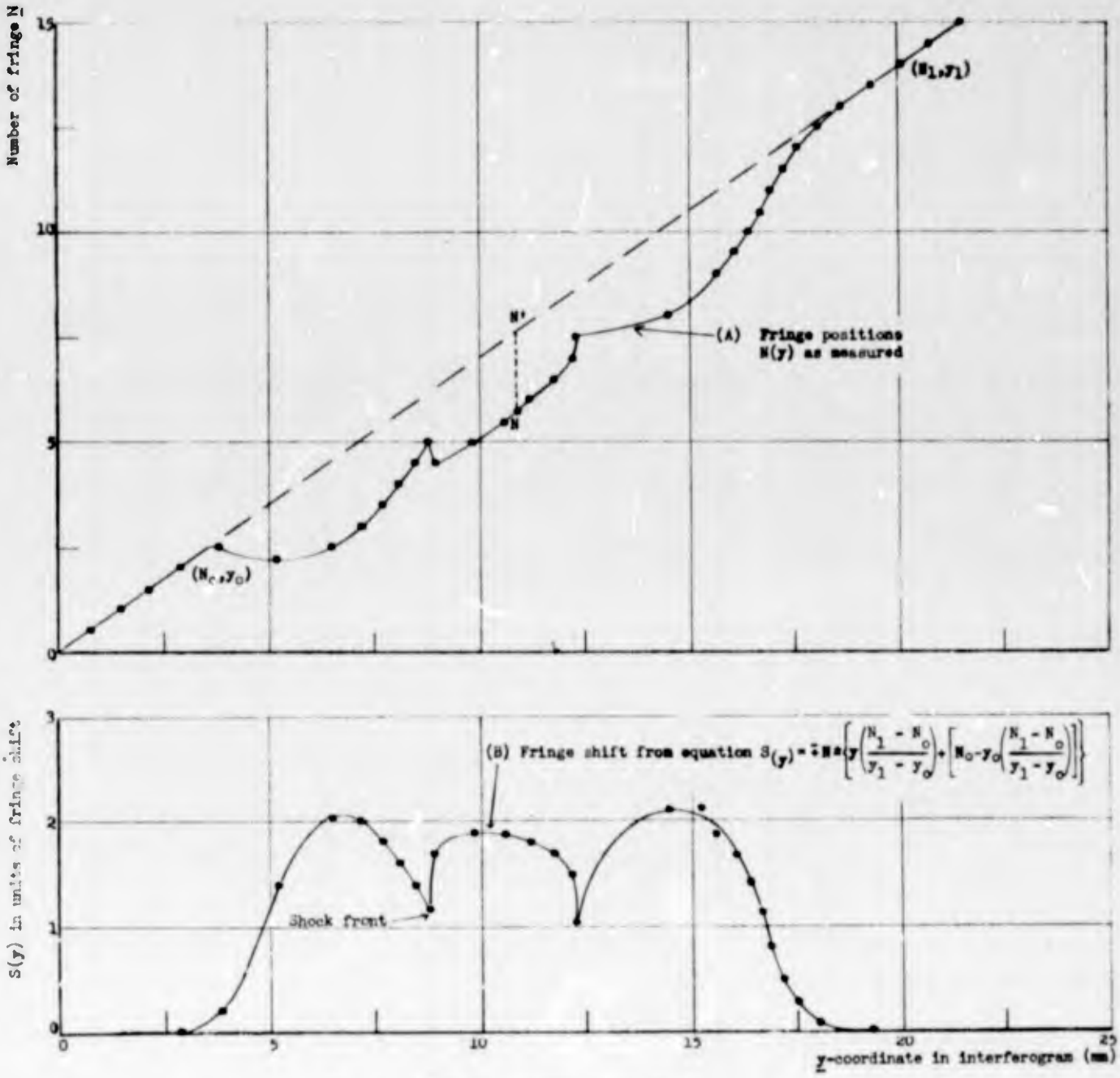

Fig. 12. Method of plotting fringe shifts.

in the same cross section, by comparing y_1 and y_o at neighboring cross sections, or some other similar means. The sign is to be chosen so that positive fringe shifts result from retarded rays, where the average density through the jet is greater than in the undisturbed beam.

It is assumed in the foregoing discussion that the undisturbed fringes are uniformly spaced, as shown by the dashed line in Fig. 12(A), which is not strictly true because the surfaces of the interferometer plates are not absolutely plane. However we have measured plates containing only undisturbed fringes, and find that this effect may be neglected over the region covered by the jet.

A smooth curve is drawn through the points $[y, S(y)]$, except where shock fronts produce a discontinuity in the derivative.

3. Calculation of density from fringe shifts

If the density pattern under investigation is one or two dimensional, Eq. (1), Part III, Sec. 2, becomes simply

$$n(x) - n_o = \frac{S(y)\lambda}{\ell} \qquad (6a)$$

where n_o is the refractive index of the room air, and the density follows from Eq. (2). If the density pattern is three dimensional, and is symmetrical about an axis, as in the case of our gas jets from a round orifice, Eq. (1) becomes

$$s(y) = \frac{2}{\lambda} \int_y^R (n(r) - n_o) \frac{r\, dr}{\sqrt{r^2 - y^2}}, \qquad (6b)$$

where $r^2 = x^2 + y^2$ and R is the radius of the jet.

Equation 6-b has the form of Abel's integral equation. The evaluation of n(r) may be accomplished either by solving the equation by a method of inversion, and then applying a numerical calculation to the result, or by approximating the equation as it stands. The various methods of solution are discussed by F. J. Weyl (18-b).

Schardin (17-F) made use of the latter method 6/ and assumed that each cross section in the circularly symmetric pattern was divided up into concentric rings, in each of which the density was assumed constant. The effect of the outer ring was calculated first, from the known chord length and fringe shift at y=R. The effect of this ring was then subtracted away from the observed effect on the next inner chord, and the second ring was evaluated, and so on. Thus a staircase radial density function is the final result. C. C. Van Voorhis of Palmer Laboratory made a more accurate assumption, namely, that the density increases linearly between zones. This idea was expressed in its present mathematical form by Dr. F. J. Weyl of the Navy Department, Bureau of Ordnance. The procedure is as follows:

Let

$$n(r) - n_o = \nu(r);$$

then Eq. (6b) becomes

$$s(y) = \frac{2}{\lambda} \int_y^R \nu(r) \frac{r\,dr}{\sqrt{r^2 - y^2}}.$$

6/ It appears that this scheme was first used by E. Mach, Von Weltrubsky and L. Mach long before Schardin's results were published (17-D).

Let the jet cross section be subdivided into zones

$$0 = r_0 < r_1 < r_2 < \ldots\ldots < r_{n-1} < r_n = R.$$

The values of $\underline{\nu}$ on the zone boundaries shall be written as

$$\nu(r_i) = \nu_i \qquad \text{for } i = 0, 1, \ldots\ldots n-1$$

$$\nu(r_i) = 0 \qquad \text{for all } i \geqq n$$

and the fringe shifts $\underline{S}$ at distances $y = r_0, r_1 \ldots\ldots$ from the jet axis will similarly be denoted by

$$S_0, S_1 \ldots\ldots S_{n-1},$$

and

$$S_n = S_{n+1} = \ldots\ldots = 0.$$

We now make the assumption that $\underline{\nu}$ varies linearly within each zone, that is,

$$\nu(r) = \nu_i + \frac{\nu_{i+1} - \nu_i}{r_{i+1} - r_i}(r - r_i) \qquad r_i \leqq r \leqq r_i$$

hence,

$$\nu(r) = \nu_i \cdot \frac{r_{i+1} - r}{r_{i+1} - r_i} + \nu_{i+1} \cdot \frac{r - r_i}{r_{i+1} - r_i}$$

Transforming the integral and inserting the $\nu(r)$ just given, we obtain

$$S_i = \frac{2}{\lambda} \sum_{\mu=i}^{n} \int_{r_\mu}^{r_{\mu+1}} \left\{ \nu_\mu \frac{r_{\mu+1} - r}{r_{\mu+1} - r_\mu} + \nu_{\mu+1} \frac{r - r_\mu}{r_{\mu+1} - r_\mu} \right\} \frac{r\,dr}{\sqrt{r^2 - r_i^2}}$$

This is readily transformed to

$$\frac{\lambda S_i}{2} = \frac{\nu_i}{r_{i+1}-r_i}\int_{r_i}^{r_{i+1}} \frac{r(r_{i+1}-r)}{\sqrt{r^2-r_i^2}}\,dr + \sum_{\mu=i+1}^{n} \nu_\mu \left\{ \frac{\int_{r_\mu}^{r_{\mu+1}} \frac{r(r_{\mu+1}-r)\,dr}{\sqrt{r^2-r_i^2}}}{r_{\mu+1}-r_\mu} - \frac{\int_{r_{\mu-1}}^{r_\mu} \frac{r(r_{\mu-1}-r)\,dr}{r_\mu - r_{\mu-1}}}{r_\mu - r_{\mu-1}} \right\}$$

$$= \nu_i A_i + \sum_{\mu=i+1}^{n} \nu_\mu A_{\mu,i}$$

The coefficients of ν_i and ν_μ may be further reduced, resulting in

$$A_i = \int_{r_1}^{r_i} \frac{\sqrt{r^2-r_i^2}}{r_{i+1}-r_i}\,dr,$$

and

$$A_{\mu,i} = \int_{r_i}^{r_{i+1}} \frac{\sqrt{r^2-r_i^2}}{r_{\mu+1}-r_\mu}\,dr - \int_{r_{\mu-1}}^{r_\mu} \frac{\sqrt{r^2-r_i^2}\,dr}{r_\mu - r_{\mu-1}}$$

Now

$$\int_{r_\mu}^{r_{\mu+1}} \sqrt{r^2 - r_i^2}\, dr = \frac{1}{2}\left\{ K(r_i, r_{\mu+1}) - K(r_i, r_\mu)\right\}.$$

where $K(p,g) = \epsilon\sqrt{g^2 - p^2} \quad - p^2 \log\left(g\sqrt{g^2 - p^2}\right)$.

It follows that the system of equations to be solved for the ν_μ is

$$\lambda S_i = \nu_i \frac{K(r_i, r_{i+1}) - K(r_i, r_i)}{r_{i+1} - r_i}$$

$$+ \sum_{\mu=i+1}^{n} \nu_\mu \left\{ \frac{K(r_i, r_{\mu+1}) - K(r_i, r_\mu)}{r_{\mu+1} - r_\mu} - \frac{K(r_i, r_\mu) - K(r_i, r_{\mu-1})}{r_\mu - r_{\mu-1}} \right\}$$

If all zones are of equal width ω, this becomes

$$S_i = \nu_i' \left[K(i, i+1) - K(i, i) \right] + \sum_{\mu=i+1}^{n} \nu_\mu' \left[K(i, \mu+1) - 2K(i, \mu) + K(i, \mu-1) \right],$$

where

$$\nu_i' = \frac{\omega \nu_i}{\lambda}.$$

The procedure was to calculate the coefficients,

$$a_{i,\mu} = K(i,\mu+1) - K(i,\mu)$$
$$= (\mu+1)\sqrt{(\mu+1)^2 - i^2} - \mu\sqrt{\mu^2 - i^2}$$
$$- i^2 \log \frac{(\mu+1)\sqrt{(\mu+1)^2 - i^2}}{\mu + \sqrt{\mu^2 - i^2}}, \quad (7)$$

and to draw up a master table for calculating the ν's. The beginning of the master table is shown in Table I. A complete master table of the coefficients $a_{i,i}$ and $b_{i,\mu}$ where $b_{i,\mu}$ $a_{i,\mu} - a_{i,\mu-1}$ for 50 zones is given as the Appendix to this report.

The calculation of the $\underline{\nu}'$ values then proceeds as shown in Table II (example with six zones), which is the same in form as Schardin's method as discussed in reference 17-F. The width $\underline{\omega}$ of the zones and their number $\underline{n}$ is adjusted in accordance with the curve of fringe shifts as obtained from the interferograms so that $S_n = 0$ and therefore $\nu'_n = 0$, and S_{n-1} and ν'_{n-1} have a finite value. For the example in Table II, $n = 6$ and $S_6 = \nu'_6 = 0$. The value of ν'_6 is obtained by dividing S_5 by a_{55} and is then multiplied successively by the coefficients b_{45}, b_{35}, b_{25}, b_{15} and b_{05}, and the results set in the table as shown. The value of ν'_4 is next calculated from $(S_4 - {}_5b_{45})/a_{44}$, the result multiplied across, and so on. The symbol Σ_n in the table means the summation of all the terms appearing above this entry in the column for S_n.

Table I. Beginning of Van Voorhis-Weyl table of coefficients.

i / μ		0		1		2		3
0	a_{00}							
1	a_{01}	$a_{01}-a_{00}=b_{01}$	a_{11}					
2	a_{02}	$a_{02}-a_{01}=b_{02}$	a_{12}	$a_{12}-a_{11}=b_{12}$	a_{22}			
3	a_{03}	$a_{03}-a_{02}=b_{03}$	a_{13}	$a_{13}-a_{12}=b_{13}$	a_{23}	$a_{23}-a_{22}=b_{23}$	a_{33}	
4	a_{04}	$a_{04}-a_{03}=b_{04}$	a_{14}	$a_{14}-a_{13}=b_{14}$	a_{24}	$a_{24}-a_{23}=b_{24}$	a_{34}	$a_{34}-a_{33}=b_{34}$
5	a_{05}	$a_{05}-a_{04}=b_{05}$	a_{15}	$a_{15}-a_{14}=b_{15}$	a_{25}	$a_{25}-a_{24}=b_{25}$	a_{35}	$a_{35}-a_{34}=b_{35}$

Table II. Calculation of refractive indices from fringe shifts, example for six zones.

S_0	S_1	S_2	S_3	S_4	S_5	$S_6 = 0$
$\nu'_1 b_{01}$						Outer Circumference of Jet
$\nu'_2 b_{02}$	$\nu'_2 b_{12}$					
$\nu'_3 b_{03}$	$\nu'_3 b_{13}$	$\nu'_3 b_{23}$				
$\nu'_4 b_{04}$	$\nu'_4 b_{14}$	$\nu'_4 b_{24}$	$\nu'_4 b_{34}$			
$\nu'_5 b_{05}$	$\nu'_5 b_{15}$	$\nu'_5 b_{25}$	$\nu'_5 b_{35}$	$\nu'_5 b_{45}$		
$\nu'_6 b_{06} = 0$	$\nu'_6 b_{16} = 0$	$\nu'_6 b_{26} = 0$	$\nu'_6 b_{36} = 0$	$\nu'_6 b_{46} = 0$	$\nu'_6 b_{56} = 0$	
Σ_0	Σ_1	Σ_2	Σ_3	Σ_4	$\Sigma_5 = 0$	
$S_0 - \Sigma_0$	$S_1 - \Sigma_1$	$S_2 - \Sigma_2$	$S_3 - \Sigma_3$	$S_4 - \Sigma_4$	S_5	
a_{00}	a_{11}	a_{22}	a_{33}	a_{44}	a_{55}	
$\nu'_0 = \frac{S_0-\Sigma_0}{a_{00}}$	$\nu'_1 = \frac{S_1-\Sigma_1}{a_{11}}$	$\nu'_2 = \frac{S_2-\Sigma_2}{a_{22}}$	$\nu'_3 = \frac{S_3-\Sigma_3}{a_{33}}$	$\nu'_4 = \frac{S_4-\Sigma_4}{a_{44}}$	$\nu'_5 = \frac{S_5}{a_{55}}$	$\nu'_6 = 0$

Thus

$$\Sigma_3 = \gamma_4' b_{34} + \gamma_5' b_{35} + \gamma_6' b_{36}$$
$$= \gamma_4' b_{34} + \gamma_5' b_{35}$$

since $\gamma_6' b_{36} = 0$ in this example.

It is clear that the greater the number of zones used to reduce a given fringe-shift curve, the greater will be the sensitivity to small details. Instead of using narrow zones throughout, a labor-saving procedure is to subdivide the particular zone in which the detail exists on the S(y) curve. The coefficients to be used for subdivided zones can be computed from the master table itself, with the limitation that if the nth zone is to be divided into p equal sub-zones, then the original master table coefficients must be known up to values $i, \mu = np-1$ of the indices involved.

With subdivision of zones, it has been possible in practice to increase the resolution of the reduction process to 0.06 mm, which is especially useful at shock fronts. The actual shock front (about 1 wavelength in thickness) is beyond the resolution of optical methods.

Consider the case where the zone whose inner boundary is denoted by $i = j$ is to be subdivided into p equal sub-zones. Here also $r_i = i$ for all i, if in the fractional zones $i = j + \frac{\pi}{p}$, $\pi = 1, 2, \ldots . p$.

The resulting values for the differences

$$\frac{K(r_i, r_{\mu+1}) - K(r_i, r_\mu)}{r_{\mu+1} - r_\mu}$$

will be

1. $i \leqq \mu \leqq j-1$: $\dfrac{K(r_i, r_{\mu+1}) - K(r_i, r_\mu)}{r_{\mu+1} - r_\mu} = K(i, \mu+1) - K(i, \mu)$

2. $i \leqq j$; $\mu = j + \frac{\pi}{p}$, $\pi = 0, 1, \ldots, p-1$: $\dfrac{K(r_i, r_{\mu+1}) - K(r_i, r_\mu)}{r_{\mu+1} - r_\mu}$

$$= \frac{K(ip, jp+\pi+1) - K(ip, jp+\pi)}{p}$$

3. $i = j + \frac{\pi}{p}$, $\mu = j + \frac{\pi'}{p}$, $1 \leqq \pi < \pi' \leqq p-1$: $\dfrac{K(r_i, r_{\mu+1}) - K(r_i, r_\mu)}{r_{\mu+1} - r_\mu}$

$$= \frac{K(jp+\pi, jp+\pi'+1) - K(jp+\pi, jp+\pi')}{p}$$

4. $i = j + \pi/p$, $\mu \geqq j+1$, $1 \leqq \pi \leqq p-1$: $\dfrac{K(r_i, r_{\mu+1}) - K(r_i, r_\mu)}{r_{\mu+1} - r_\mu}$

$$= \sum_{\nu=\mu p}^{\mu p+p-1} \frac{K(jp+\pi, \nu+1) - K(jp+\pi, \nu)}{p^2}$$

5. $i, \mu \geqq j+1$: $\dfrac{K(r_i, r_{\mu+1}) - K(r_i, r_\mu)}{r_{\mu+1} - r_\mu} = K(i, \mu+1) - K(i, \mu)$

6. $i \leqq j$, $\mu \geqq j+1$: $\dfrac{K(r_i, r_{\mu+1}) - K(r_i, r_\mu)}{r_{\mu+1} - r_\mu} = K(i, \mu+1) - K(i, \mu)$

Regions 1, 5 and 6 are identical with the master table values.

Table III gives an example of a table of coefficients for 6 zones in which the 4th (between r = 3 and r = 4) is subdivided into 4 equal zones.

Geometrically, a given cross section through our gas jet may be represented by a three-dimensional model, in which $r = \sqrt{x^2 + y^2}$ is the radius, and $z = \nu'(r)$ is the excess of the refractive index over that of the outside air, times a constant. Our method of analysis then considers this model to be built up of overlapping rings of triangular cross section. The base of the ring $\underline{i}$ extends from r = i - 1 to r = i + 1. The apex of the ring, where $\nu' = \nu_i'$, is at r = i. The overlapping portions of two adjacent rings, for example i and i + 1, add up to produce a linear increase of $\underline{\nu}'$ between r = i and r = i + 1.

The coefficients in the master table represent, aside from a numerical constant, the area of intersection of such triangular rings of unit $\underline{\nu}'$ with planes parallel to the $\underline{xz}$-plane, and passed through the model of the cross section at distances, y = 0, 1,2,111 n units from the $\underline{xz}$-plane.

Schardin's method builds the jet sections up of rings of rectangular cross section, each rectangle having a base extending from r = i to r = i + 1, and a height $z = \nu_i'$. Schardin's coefficients are then merely proportional to the chord length through each ring at a distance $\underline{y}$ from the $\underline{xz}$-plane.

The shape of a Schardin zone, being a density plateau with a flat top and square front, approximates closely

Table III. Example of auxiliary table of coefficients for subdivided zones.

(Zone between r = 3 and r = 4 divided into four equal sub-zones)

μ \ i	0		1		2		3		$3\frac{1}{4}$		$3\frac{2}{4}$		$3\frac{3}{4}$		4		5	
		Δ^2K		Δ^2K		Δ^2K		Δ^2K		Δ^2K		Δ^2K		Δ^2K		Δ^2K		Δ^2K
0	a_{00}	Differences		Differences		Differences		Differences		Differences		Differences		Differences		Differences		
1	a_{01}		a_{11}															
2	a_{02}		a_{12}		a_{22}													
3	$\frac{1}{4}a_{0,12}$		$\frac{1}{4}a_{4,12}$		$\frac{1}{4}a_{8,12}$		$\frac{1}{4}a_{12,12}$											
$3\frac{1}{4}$	$\frac{1}{4}a_{0,13}$		$\frac{1}{4}a_{4,13}$		$\frac{1}{4}a_{8,13}$		$\frac{1}{4}a_{12,13}$		$\frac{1}{4}a_{13,13}$									
$3\frac{2}{4}$	$\frac{1}{4}a_{0,14}$		$\frac{1}{4}a_{4,14}$		$\frac{1}{4}a_{8,14}$		$\frac{1}{4}a_{12,14}$		$\frac{1}{4}a_{13,14}$		$\frac{1}{4}a_{14,14}$							
$3\frac{3}{4}$	$\frac{1}{4}a_{0,15}$		$\frac{1}{4}a_{4,15}$		$\frac{1}{4}a_{8,15}$		$\frac{1}{4}a_{12,15}$		$\frac{1}{4}a_{13,15}$		$\frac{1}{4}a_{14,15}$		$\frac{1}{4}a_{15,15}$					
4	$a_{0,4}$		$a_{1,4}$		$a_{2,4}$		$a_{3,4}$		$\frac{1}{16}\sum_{16}^{19} a_{13,\mu}$		$\frac{1}{16}\sum_{16}^{19} a_{14,\mu}$		$\frac{1}{16}\sum_{16}^{19} a_{15,\mu}$		$a_{4,4}$			
5	$a_{0,5}$		$a_{1,5}$		$a_{2,5}$		$a_{3,5}$		$\frac{1}{16}\sum_{20}^{23} a_{13,\mu}$		$\frac{1}{16}\sum_{20}^{23} a_{14,\mu}$		$\frac{1}{16}\sum_{20}^{23} a_{15,\mu}$		$a_{4,5}$		$a_{5,5}$	

Note: The entry in the Δ^2K column at (i,μ) is obtained by subtracting from the ΔK value at (i,μ) the ΔK in the line above.

BLANK PAGE

the density behind an actual shock front. It is possible, by using suitable coefficients, to insert a Schardin zone just at the shock position. It has been found that this procedure eliminates "overshooting" and produces a smooth behavior of the density curve after a shock.

4. Test of evaluation method using a hypothetical density distribution.

We have computed without approximation the fringe shift to be expected from a simple assumed density distribution, similar to those encountered in the actual gas jets studied in this report. The density was then recalculated from the fringe-shift curve by our regular method, using the Van Voorhis-Weyl table of coefficients. Figure 13 shows the assumed and final densities, and the corresponding fringe-shift curve. The recalculated result agrees well with the assumed distribution except at the shock, where the recalculated values "overshoot" and oscillate about the correct value a few times before settling down. This "overshooting" arises whenever the actual rate of change of ν in a zone is greater than the assumed linear rate between zone boundaries. Similar "overshooting" is actually observed in the density distribution obtained from cross sections in gas jets where shocks exist. (See Fig. 16)

5. Accuracy and sensitivity

For a one- or two-dimensional density pattern, the error in the final density value can be obtained by combining

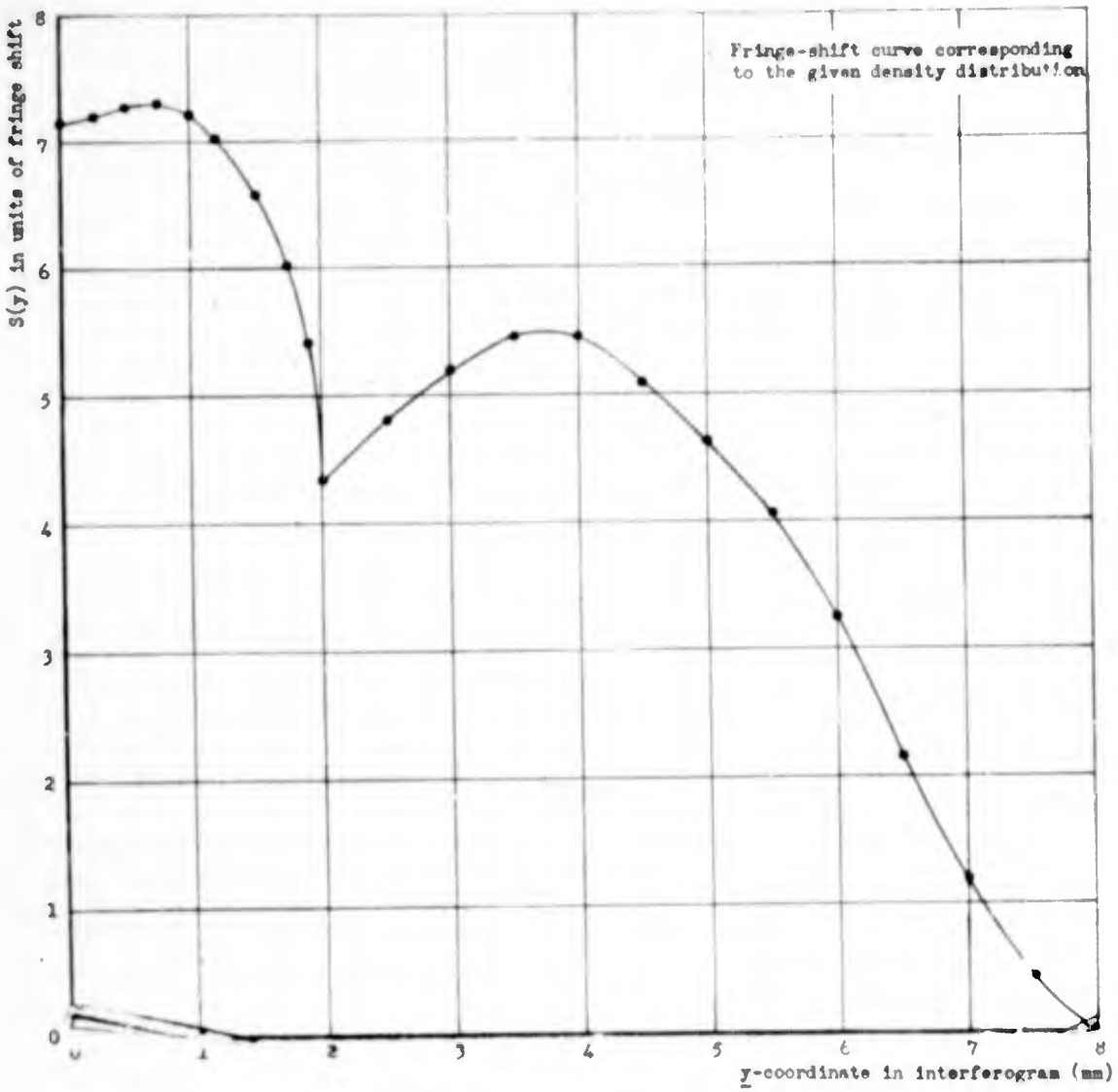

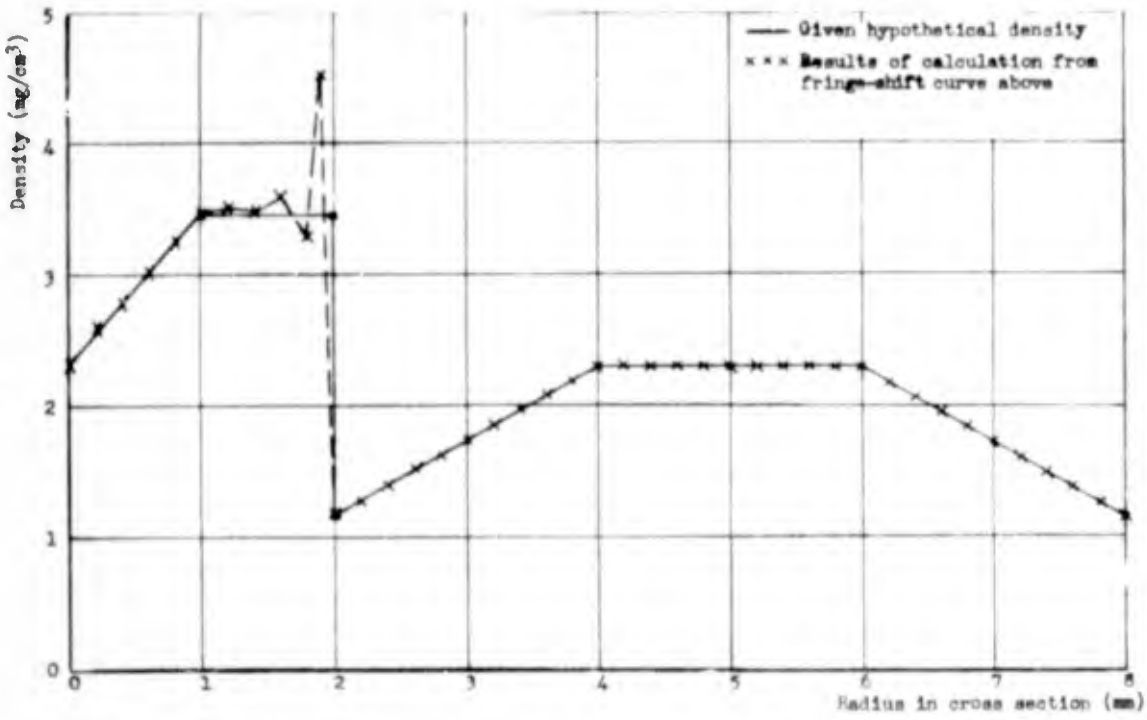

Fig. 17. Test of the method of density evaluation with a hypothetical density distribution.

Eqs. (2) and (6a) to give

$$\rho_j - \frac{K_o \rho_o}{K_j} = \frac{S(y)\lambda}{K_j \ell}$$

where K_j and K_o are the values of the Gladstone-Dale constant which apply to the jet (dry air) and to the room (wet air) respectively and

$$\Delta\rho_j = \Delta S(y)\frac{\lambda}{K_j \ell} + \frac{\Delta\rho_o K_o}{K_j}$$

For the case of a jet with circular symmetry, Eq. (6b) must be used. An estimate of the error is complicated by the stepwise, accumulative method of evaluating n(r) from Eq. (6b).

The plotted S(y) values probably represent the optical effect of the jet accurately within about 0.03 of a fringe-shift unit at places of small slope, and within 0.07 at places of large slope. The effect of this uncertainty on the density can be seen from the relation

$$\nu_i' = \frac{\nu_i \omega}{\lambda} = \frac{K_j \omega}{\lambda}(\rho_j)_i = \frac{S_i - \sum_{\mu=i+1}^{n} \nu_\mu b_{i\mu}}{a_{ii}}$$

If we assume that the error occurs in a small region, only S_i is incorrect, and the sum is unaffected. Then

$$(\Delta\rho_j)_i = \frac{\Delta S_i \lambda}{a_{ii} K_j \omega} \qquad (8)$$

In the extreme case of large slope, if the error occurs at the jet center, $a_{ii} = 1$ and with the following constants: K_j (Gladstone-Dale Constant) $= 0.2268_5$ cm^3/g (for dry air, $\lambda = 5461$ Å); λ (Light Wavelength) $= 5461$ Å; ω(Zone Width) $= 0.02$ cm; $\Delta S_i = 0.07$; the value of $\Delta\rho_i$ is given by $\Delta\rho_i = 0.8$ mg/cm^3.

If the same error occurs near the edge of the jet, $a_{ii} = a_{40,40} = 11.9703$ and

$$\Delta\rho_i = 0.07 \text{ mg/cm}^3$$

Usually, however, the S(y) curve is horizontal at the jet center, so the smaller error in S(y), 0.03, should apply. Furthermore, the S(y) curve is smoothed so that the error is spread over neighboring zones, enters into the sum, and tends to reduce itself.

Probably the major source of error arises from local fluctuations in the jet density, which disturb its cylindrical symmetry, and from random fluctuations in the density of the room air in the interferometer beams. (See Part VI-8 for moving film records of this jet) A safe limit for the absolute error is 10 percent. Density values are probably self-consistent within 5 percent.

We have attempted to estimate the minimum shock strength necessary to produce an effect in the fringe-shift curve definitely assignable to a shock, and which would accordingly be treated as such in the reduction process. It can be shown that a shock front produces a discontinuity and an infinite value of the S(y)-curve tangent, but in the case of weak shocks this may escape notice, and only the general trend of the S(y) curves on either side of the shock-front position indicate the presence of the discontinuity.

The fringe shifts S'(y) to be expected from a shock of radial density distribution $\rho'(r) = \text{const.}$, $0 \leq r \leq R$; $\rho'(r) = 0$, $r > R$ were determined under conditions

of circular symmetry as in our jets. Section of typical S(y) curves were selected, of slope -1 in case A (see Table IV), of slope 0 in case B, and of slope +1 in case C. To each measured S(y) point on these sections was then added the appropriate S'(y) value, which in effect superposed the small shock on the otherwise smooth S(y) curve.

Table IV lists the minimum ρ' which produces a fringe-shift effect assignable to a shock, under the conditions of resolution and judgment we have attained, expressed as a function of the shock-front radius R, for cases of different S(y)-curve slope.

Table IV. Calculated minimum ρ' which produces a fringe-shift effect assignable to a shock under the conditions of resolution and judgment attained in these experiments.

Distance of Shock Front from Axis (mm)	Shock Density Increment ρ' (mg/cm^3)		
	A: slope -1	B: slope 0	C: slope +1
0.1	1.0	0.8	0.6
1	0.3	.25	.2
10	.09	.08	.07
100	.03	.03	.02

6. Amount of labor required to reduce a cross section

Our method requires about 17 man-hours to analyze one cross section, broken down as follows:

1.	Measure one cross section in interferogram (100 fringes); outer parts, maxima only, twice; inner parts, maxima and minima, three times	1½ hr
2.	Average data, calculate and plot fringe shifts	2 hr
3.	Tabulate average $\underline{S}$ values at zone boundaries	1 hr
4.	Prepare auxiliary table of coefficients, with certain zones subdivided (not always required)	4 hr
5.	Compute $\underline{\nu}'$ values, using 30 to 40 zones	8 hr
6.	Compute ρ values	½ hr
	Total time	17 hr

The method of reduction which uses the exact solution of the Abel integral equation for the fringe shift combined with the use of business machines for speeding up the calculating, is in use at the Navy Department, Bureau of Ordnance, Washington, D. C. By using machine multiplication, and running up to ten cross sections at once, part 4 is eliminated, and much time is gained in part 5. This latter method has been applied by the Navy Department to the fringe-shift curves for the 10-S-60 jet described in the next section, and the results are in exact agreement with the present results except at shock fronts, where the method does not oscillate but settles down uniformly after the first "overshooting". However, a method of "deshocking" has been developed which removes this behavior, and can be applied in special cases. (See Weyl's report 18b) The Navy Department method is useful for evaluating large quantities of data, whereas the method in use at Princeton is useful for obtaining high resolution in isolated cross sections by subdividing the zones.

1. Shadowgrams of an air jet at various pressures

Figure 14 shows shadowgrams of the air jet from the 10 mm orifice at reservoir pressures of 20, 40, 60, 80, and 110 lbs/in^2 overpressure, made as described in Section IV - 2. The jet escapes upward from the orifice (black shadow at bottom).

These photographs clearly reveal the characteristic development of the shock formations and jet expansion as produced by the increasing reservoir - receiver pressure ratio. In A the jet emerges nearly at atmospheric pressure and undergoes little expansion. A weak conical shock arises at the edge of the orifice, converges, crosses with a simple interaction, and diverges, to be reflected at the free boundary at the end of the first "period" of the jet. In B the jet expands more, resulting in a strengthening of the conical shock near the crossing point. In this case the simple X interaction is about to break over into the Y interaction, which is shown fully developed in case C. D and E represent further stages, in which the jet expands a great deal. The normal shock appears curved, but this may be partly optical distortion. The streaks in these shadowgrams which appear like streamlines are probably the trail of vortices formed at the boundary of the jet, and which move an appreciable distance during the time of illumination.

Another feature revealed by shadowgrams is the vortex sheet or slip stream, representing the boundary between two gas

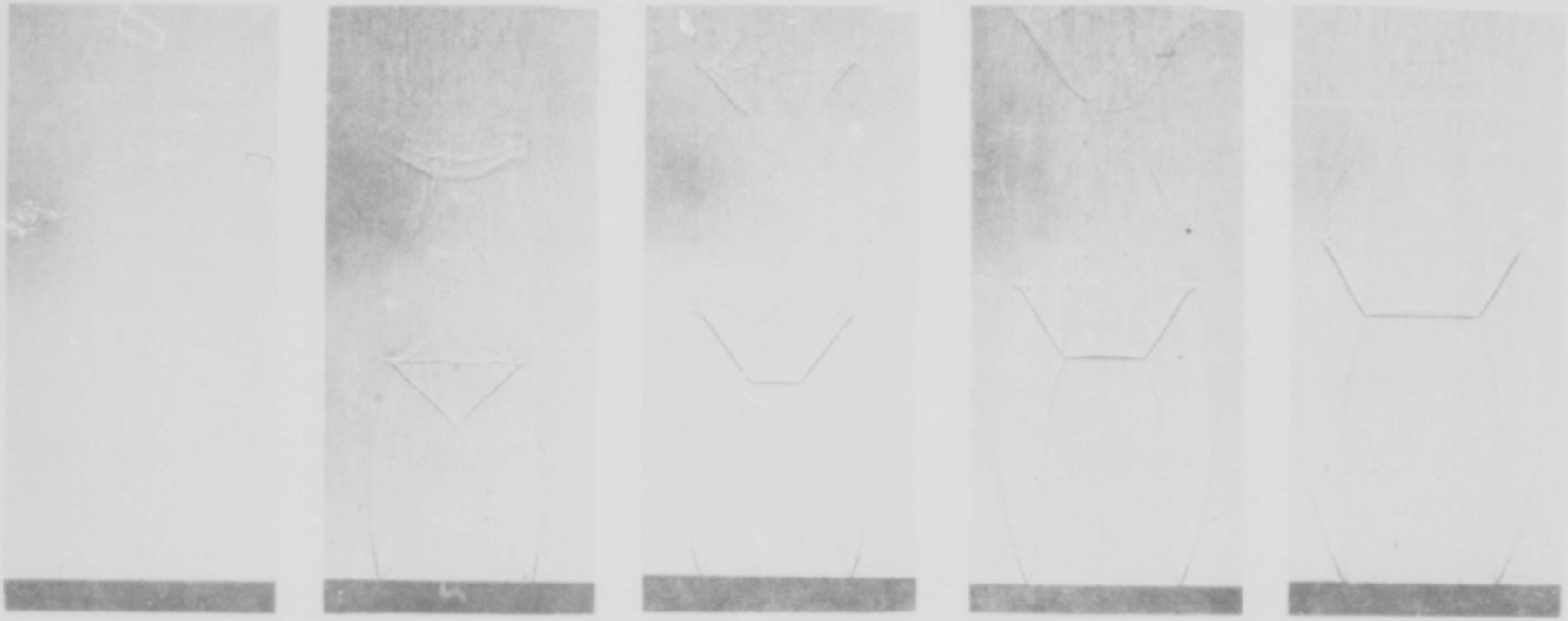

A - 20 B - 40 C - 60 D - 80 E - 110

Fig. 14

Shadowgrams of Air Jets at Various Reservoir Pressures

BLANK PAGE

streams flowing parallel with the same pressure, but having different density and velocity. This line can be seen originating from the "triple point" in Figure 14 - C, D, and E, where the conical and normal shocks intersect.

2. Interferogram of an air jet at 60-lb/in.^{2} pressure (10-S-60 jet).

Figure 15 is an interferogram of an air jet from the streamlined orifice described in Fig. 10, at a tank pressure of 60 lb/in.^{2} over atmospheric (hereafter designated as 10-S-60 jet). The jet is located in one arm of the interferometer as shown in Fig. 2. This interferogram corresponds to the shadowgram of figure 14-C.

The fringes are oriented parallel to the jet axis, are spaced about 0.2 mm and have a virtual location in a plane through the jet axis normal to the light beam. The interferogram appears unsymmetrical as the fringes shift to the right if the integrated density through the jet at a given Y value is higher than atmospheric. Since the jet is symmetrical, this produces a crowding of the fringes on the right, and a widening on the left. The movement of fringes from their undisplaced position is the same for symmetrical points in the jet, however. The light source used was described in Part III, Sec. 5-ii. This source gives sufficiently parallel light. The interferogram reveals the shock waves in the same positions as the shadowgram, by sudden displacements of the fringes. The shocks have been numbered for reference.

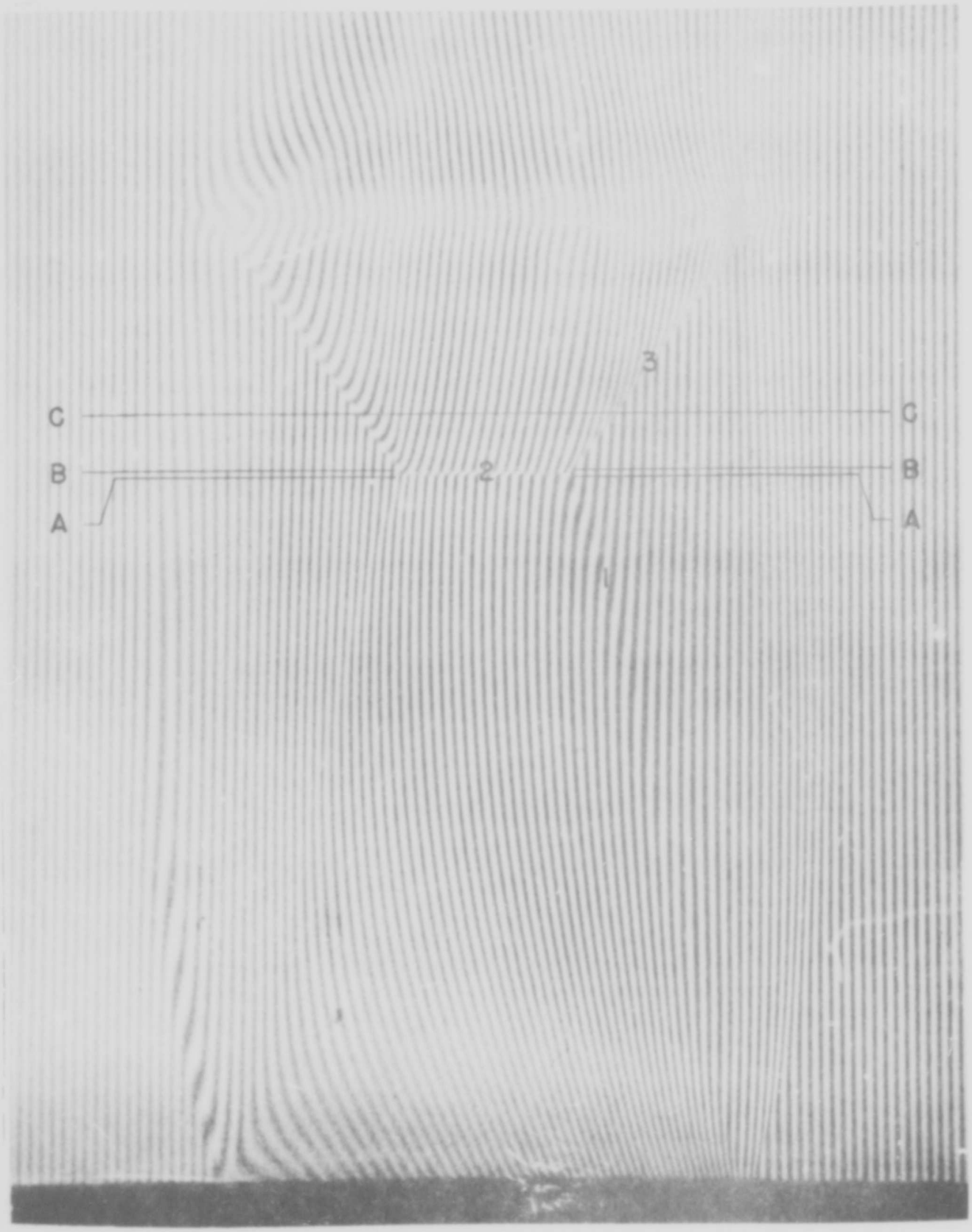

Fig. 15. Interferogram of the 10-S-60 air jet, magnification 9 times.

Shock 2 appears to be shaped like an inverted saucer or dome. This dome effect is even more pronounced at high tank pressures.

Shock 1 apparently originates at the edge of the orifice, although it is very weak there. Both 1 and 3 are sections of conical shocks in the circular jet, joining shock 2 at the "triple point".

3. Fringe shifts and density cross sections in the shock region.

Figure 16 gives three curves of fringe-shift values and the resultant radial density distribution in the section A-A, B-B, and C-C of Fig. 15. The zones used for reducing the S values to densities are shown by the points on the density plots. The reduction was carried out using the VanVoorhis-Weyl master table of coefficients in the manner outlined in Part V, Sec. 3. Frequent subdivision of the zones into thirds of quarters was used across shock fronts to improve the resolution.

In the equation for the jet density ρ_j

$$\rho_j = \frac{\nu}{K_j} + \rho' \qquad (9)$$

where $\nu = n_j - n_o$ is obtained from the numerical evaluation, the constants had the following values

λ	(Light wavelength)	$= 5.461 \times 10^{-5}$ cm,
K_j	(Gladstone-Dale constant for air[7/])	$= 0.22685$ cm^3/gm
ω	(Zone width)	$= 0.02$ cm,
ρ'	(Equivalent density of room air, assumed half-saturated)	$= 1.176$ mg/cm^3.

7/ Selected from best critical table values of index of refraction and density for air.

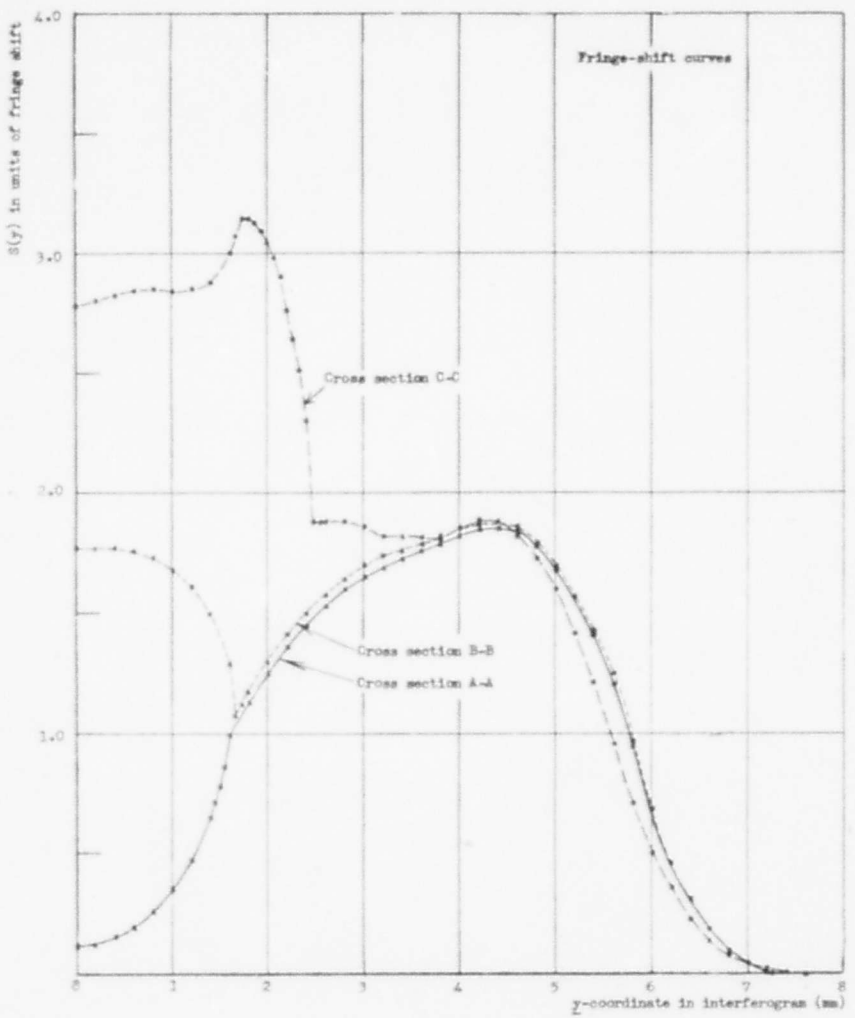

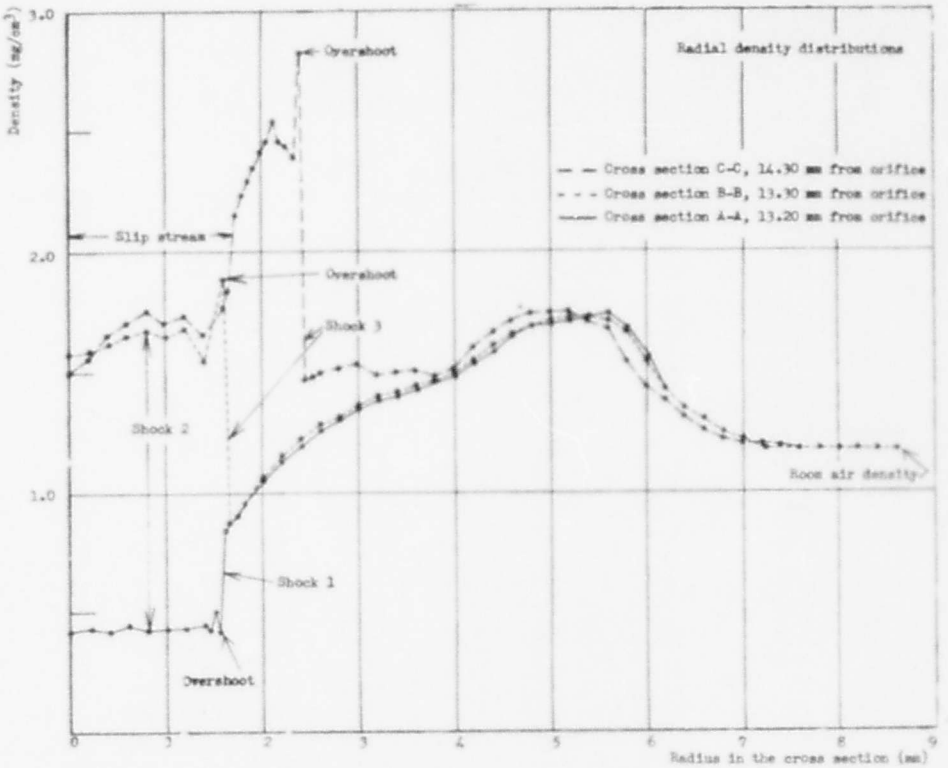

Fig. 16. Fringe shifts and density cross sections for the 10-3-60 jet.

BLANK PAGE

Tank conditions were as follows:

$$\rho_o = 6.06 \text{ mg/cm}^3,$$
$$P_o = 5.08 \text{ atm},$$
$$T_o = 297^\circ\text{K}.$$

The cross sections A-A and B-B were measured on each side of the shock 2 as close to it as possible. The densities in A-A and B-B do not differ appreciably outside the shock region, where the z-density gradient is small. Section A-A crosses shock 1, and section B-B shock 3. The sudden rise of density in shock 3 occurs in a radial distance less than 0.06-mm as shown by the overshooting at the calculated point in the 0.06 mm wide zone. Similarly, shock front 1, although weaker and reversed from shock 3, occurs in a radial distance of less than 0.05 mm.

The jump in density across shock 2 can be obtained from the axial regions of density in A-A and B-B. Density section C-C shows an abrupt rise at shock 3, which occurs now at a greater distance from the axis than in B-B, and then a sharp drop at the boundary of the slip stream between air flowing at subsonic velocity after traversing shock 2, and air which crosses 1 and 3, and remains supersonic. Comparison of shock strengths with theory is given in Part VI, Sec. 6.

4. Density near jet axis as a function of z

Thirty-five cross sections were measured in the interferogram of Fig. 15; one group spaced 1 mm between orifice and shock 2; another group of six, three on each side of shock 2, spaced 0.1 mm; then a series spaced 0.5 mm covering the

remainder of the plate. The group of six near shock 2 was averaged over the two sides of the jet. In other sections, values from half the jet only were used for reduction.

Fig. 17 is a plot of the density along a line 1 mm from the jet axis as a function of distance z from the orifice. The axial values are practically the same as this curve, but fluctuate more owing to the lower accuracy at r = 0.

The jet undergoes an expansion in the region between 0 and 13.2 mm, at the same time accelerating, up to shock 2. The shock front occurs in an interval less than 0.1 mm, after which the gas compresses slightly, reaches very low velocity, and then begins a second expansion and acceleration after z = 19 mm. Pressure, temperature, Mach number and velocity as functions of density for the region between the orifice and shock 2 are given in Table V, and after shock 2 in Table VI.

In the supersonic region between the orifice and shock 2, an increase in the cross-sectional area A produces a decrease in the density ρ, but in the subsonic stream after shock 2 the reverse is true, ρ increases with A. This is clearly shown in Fig. 20 for the slip stream occurring after shock 2 expands, corresponding to the increase of density from ρ = 1.65 mg/cm^3 at z = 13.3 mm, to ρ = 1.80 mg/cm^3 at z = 18.5 mm (see Fig. 17).

This can be understood theoretically from the

BLANK PAGE

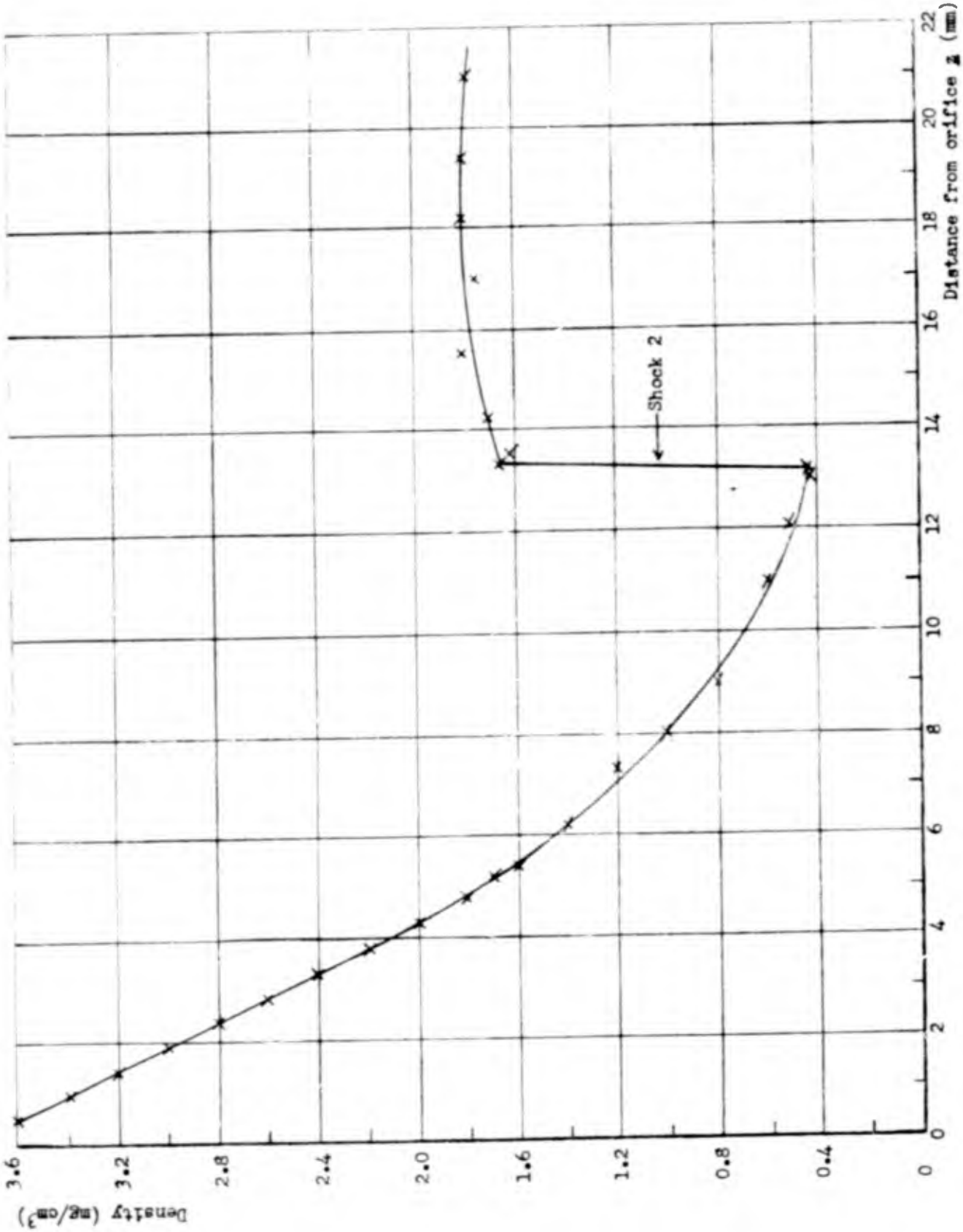

Fig. 17. Density as a function of z, 1 mm from jet axis.

equation

$$\frac{dA}{A} = \frac{d\rho}{\rho}\left(\frac{a^2}{u^2} - 1\right)$$

(where a is the velocity of sound and u the velocity of flow) which may be derived, assuming one-dimensional flow, from the equation of continuity,

$$A\rho u = \text{const.}$$

the momentum conservation equation,

$$u\,du + \frac{dP}{\rho} = 0,$$

and the relation for sound velocity

$$a^2 = \frac{dP}{d\rho}.$$

For $u > a$, the right side is negative, and it is positive for $u < a$.

At z = 18.5 mm the Mach number drops to a minimum value of 0.35 and the corresponding air velocity to 118 meter/sec.

5. Complete density analysis of the 10-S-60 jet

The complete density analysis of this jet is given in Fig. 18. The air density (mg/cm^3) is indicated on each isopycnal (line of constant density). The irregularities in the isopycnals are either the result of turbulence in the jet or statistical errors somewhere in the reduction process. No attempt was made to smooth the isopycnic lines.

6. Calculation of temperature, pressure, Mach number, and shock strength in the jet.

Knowledge of the density and the initial conditions

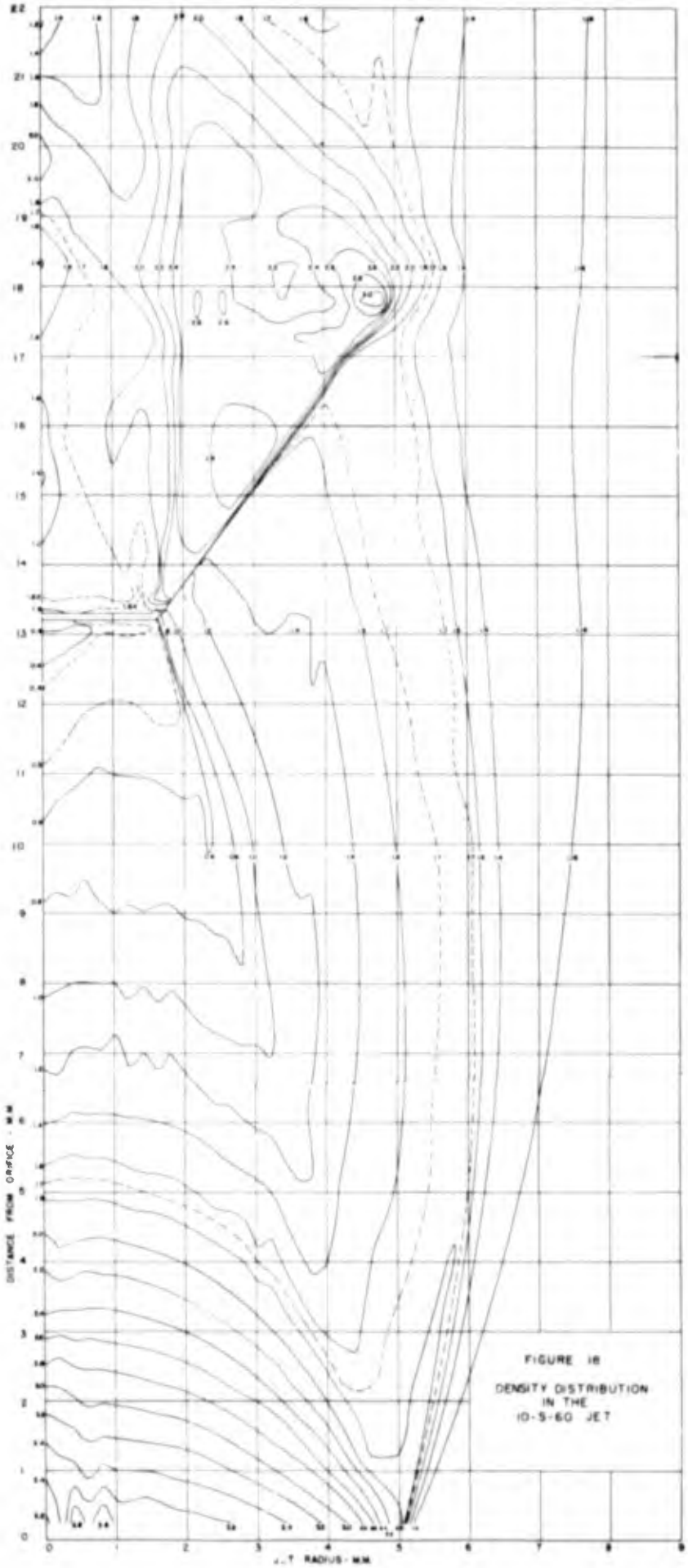

FIGURE 18

DENSITY DISTRIBUTION
IN THE
10-S-60 JET

enables one to calculate the temperature T, pressure P, Mach number M, and flow velocity V in the jet. In the region bounded by the orifice, the jet boundary, and shocks 2 and 3 the adiabatic law may be used (as shock 1 is weak) starting from the values in the tank, where V = 0. Across shocks 2 and 3, P, T, M and V are connected by the Rankine-Hugoniot equations. In the regions bounded by shock 2 and the slip stream and in the region between the slip stream and shock 3 the adiabatic law has to be used again, beginning with the conditions just after the shocks. Once the temperature is known, the Mach number may be calculated from the energy law, which holds anywhere in the jet.

$$\frac{V^2}{2} + C_p T = \text{const.} = C_p T_o \qquad (10)$$

where T_o is the tank temperature and C_p is the specific heat at constant pressure. Table V gives the temperature, pressure, Mach number, and velocity labels for each isopycnic line in the adiabatic region together with the exact initial conditions and equations used. These same quantities are given in the Table VI for the region after shock 2, and in Tables VII and VIII for two regions at different radii after shock 3.

These tables are valid only inside the 1.7 mg/cm^3 contour, due to mixing of the jet with the atmosphere outside this line.

If tables V, VI, VII, and VIII are used in conjunction with Figs. 17 and 18, it may be seen that the flow is supersonic everywhere except in the region bounded by shock 2 and the slip stream downstream from it. By further applica-

Table V. Temperature, pressure, Mach number, and velocity as adiabatic functions of density for the 10-S-60 jet.

$\frac{P}{P_o} = \left(\frac{\rho}{\rho_o}\right)^{\gamma}$; $\frac{T}{T_o} = \left(\frac{\rho}{\rho_o}\right)^{\gamma-1}$; $M^2 = \frac{v^2}{a^2} = \frac{2}{\gamma-1}\left(\frac{T_o}{T} - 1\right)$; $V^2 = 2C_p(T_o - T)$; $\gamma = \frac{C_p}{C_v} = 1.404$;

$C_p = 1.00 \times 10^7$ erg/gm°K; $\rho_o = 6.06$ mg/cm^3; $P_o = 5.08$ atm; $T_o = 297$°K.

Density ρ (mg/cm^3)	Pressure P (atm)	Temperature T (°K)	Mach Number M	Velocity V (meter/sec)
0	0	0		770
0.2	0.043	76	3.81	664
.4	.112	99	3.14	629
.6	.197	116	2.76	602
.8	.295	131	2.51	575
1.0	.409	145	2.30	551
1.2	.524	155	2.14	532
1.4	.645	164	2.00	516
1.6	.782	173	1.88	498
1.8	.929	181	1.77	482
2.0	1.078	189	1.67	465
2.2	1.225	197	1.58	447
2.4	1.398	205	1.50	428
2.6	1.552	212	1.42	412
2.8	1.730	218	1.35	397
3.0	1.883	224	1.28	382
3.2	2.065	230	1.21	366
3.4	2.26	236	1.14	350
3.6	2.44	241	1.08	334
3.8	2.63	246	1.02	319
4.0	2.80	250	0.96	306

Table VI. Pressure, temperature, Mach number, and velocity after shock 2.

$$\frac{P}{P_2} = \left(\frac{\rho}{\rho_2}\right)^{\gamma} \qquad \frac{T}{T_2} = \left(\frac{\rho}{\rho_2}\right)^{\gamma-1} \qquad V = \sqrt{2C_p(T_o - T)} \qquad M = \sqrt{\frac{2}{\gamma-1}\left(\frac{T_o}{T} - 1\right)}$$

$$\frac{P_2}{P_1} = \frac{\frac{\gamma+1}{\gamma-1} \cdot \frac{\rho_2}{\rho_1} - 1}{\frac{\gamma+1}{\gamma-1} - \frac{\rho_2}{\rho_1}} \qquad \frac{T_2}{T_1} = \frac{\frac{\gamma+1}{\gamma-1} - \frac{\rho_1}{\rho_2}}{\frac{\gamma+1}{\gamma-1} - \frac{\rho_2}{\rho_1}}$$

$P_1 = 0.121$ atm, $T_1 = 101^{\circ}K$, $C_p = 1.00 \times 10^7$ erg/gm$^{\circ}K$, $\rho_1 = 0.42$ mg/cm^3,

$\rho_2 = 1.63$ mg/cm^3 $\qquad \gamma = \frac{C_p}{C_v} = 1.404$

Density ρ (mg/cm^3)	Pressure P (atm)	Temperature T ($^{\circ}K$)	Mach Number M = V/a	Velocity V (meter/sec)
1.0	0.643	228	1.23	371
1.2	0.832	246	1.01	320
1.4	1.03	262	0.78	265
1.6	1.25	276	.59	205
1.8	1.47	290	.35	118
2.0	1.71	302	imaginary	imaginary
2.2	1.95	314	imaginary	imaginary
2.4	2.20	325	imaginary	imaginary
2.6	2.47	336	imaginary	imaginary
2.8	2.74	346	imaginary	imaginary
3.0	3.01	356	imaginary	imaginary

Table VII. Pressure, temperature, Mach number, and velocity after shock 3 at 2.8 mm from axis.

For equations used see Table VI.

Initial conditions as follows:

P_1 = 0.742 atm

T_1 = 172°K

C_p = 1.00 x 10^7 erg/gm°K

ρ_1 = 1.55 mg/cm^3

ρ_2 = 2.66 mg/cm^3

$\gamma = C_p/C_v$ = 1.404

Density ρ (mg/cm^3)	Pressure P (atm)	Temperature T (°K)	Mach Number M = V/a	Velocity V (meter/sec)
1.0	0.41	147	2.25	548
1.2	.53	157	2.10	529
1.4	.66	167	1.97	510
1.6	.80	177	1.83	490
1.8	.94	186	1.71	471
2.0	1.10	194	1.62	454
2.2	1.26	202	1.54	437
2.4	1.43	208	1.46	421
2.6	1.59	215	1.38	405
2.8	1.76	222	1.30	388
3.0	1.94	229	1.21	369

Table VIII. Pressure, temperature, Mach number, and velocity after shock 3 at 4.0 mm from axis.

For equations used see Table VI.

Initial conditions as follows:

$P_1 = 0.845$ atm $\qquad \rho_1 = 1.70$ mg/cm^3

$T_1 = 177^\circ$K $\qquad \rho_2 = 2.60$ mg/cm^3

$C_p = 1.00 \times 10^7$ erg/gm$^\circ$K $\qquad \gamma = C_p/C_v = 1.404$

Density ρ (mg/cm^3)	Pressure P (atm)	Temperature T ($^\circ$K)	Mach Number M = V/a	Velocity V (meter/sec)
1.0	0.41	144	2.30	553
1.2	.53	155	2.14	533
1.4	.65	165	1.99	514
1.6	.79	174	1.87	496
1.8	.93	183	1.76	478
2.0	1.08	191	1.66	461
2.2	1.23	198	1.57	444
2.4	1.39	205	1.49	428
2.6	1.56	212	1.41	412
2.8	1.73	218	1.34	397
3.0	1.90	224	1.27	382

tion of the laws of fluid dynamics a series of check calculations can be made as follows:

(1) The conservation of mass requires that $I = \int \rho v \, dA$ be constant for various cross sections. The computation is somewhat uncertain as the boundary of the jet is not well defined; the actual results obtained were,

$z = 0.2$ mm, $I = 91$ gm/sec;

$z = 5.0$ mm, $I = 93$ gm/sec;

$z = 10.0$ mm, $I = 91$ gm/sec.

A rough estimate obtained from the tank-pressure drop of 4 lb/in^2 in 5 sec, conducted isothermally, gives $I = 97$ gm/sec.

(2) The expected shock strength may be calculated theoretically from the Mach number in the stream using the general equation

$$\frac{\rho_2}{\rho_1} = \frac{\frac{\gamma+1}{2}}{\frac{1}{M_n^2} + \frac{\gamma-1}{2}} \qquad (11)$$

where $\frac{\rho_2}{\rho_1}$ is the density ratio across the shock, γ is the ratio of specific heats, and M_n is the upstream component of the Mach number normal to the shock front, which differs from the total Mach number if the shock is inclined to the flow direction. We find this equation to be in excellent agreement with our results, within experimental errors, as shown in the following tabulation.

Shock	M_{total}	M_n	ρ_2/ρ_1	
			Calculated	Observed
2	3.10	3.10	3.93	3.88
3	1.91	1.35	1.61	1.67

The value of M_{total} is obtained from the density ρ_1 and the initial conditions. An alternative would be to express M_n in equation (11) directly in terms of ρ_1, ρ_0 and the angle of the stream against the shock. The stream direction against the shocks was measured by bisecting the head wave of a probe, as described in the next section.

(3) A further check is obtained by calculating the density at the orifice of "throat," where, theoretically, if the flow is one dimensional the Mach number should be unity. From the corresponding relation, $\frac{\rho_1}{\rho_0} = \left(\frac{1+\gamma}{2}\right)^{\frac{1}{1-\gamma}} = 0.6342$

one obtains ρ_1 = 3.84 with ρ_0 = 6.06 mg/cm^3. Our measurements give 3.8 for the density near the axis 0.2 mm above the orifice. With increasing distance from the axis the density drops more and more, as the orifice does not give a perfectly uniform flow.

(4) An important further check of our results can be obtained by calculating the pressures at both sides of the slip stream above the "triple point", where the subsonic flow above shock 2 and the supersonic flow above shock 3 come together. These pressures should be equal. We find 1.58 and 1.50 atm, corresponding to the observed density 1.90 mg/cm^3 shock 2 (Table VI), and 2.5 mg/cm^3 at the other side of the slip stream, above shock 3 (Table VII).

(5) Finally, the entropy values at both sides of the slip stream can be calculated easily, and their differences should correspond to the densities at both sides of the slip

stream. As the entropy change is given by the relation

$$S_2 - S_1 = C_v \left(\log \frac{P_2}{\rho_2^\gamma} - \log \frac{P_1}{\rho_1^\gamma} \right) = C_v \log \frac{\xi}{\eta^\gamma} = C_v \log F,$$

where

$$\frac{P_2}{P_1} = \xi \qquad \frac{\rho_2}{\rho_1} = \eta \qquad\qquad F = \frac{\xi}{\eta^\gamma}$$

it is useful in the present case to calculate the expression

$$F^{\frac{1}{\gamma}} = \frac{\xi^{\frac{1}{\gamma}}}{\eta}$$

The observed values for η and ξ are,

for shock 2 at 1.5 mm from the axis: $\eta = \frac{1.65}{0.45} = 3.66$,

$$\xi = \frac{5.95\,\eta - 1}{5.95 - \eta} = 9.08;$$

for shock 3 at 2.0 mm from the axis: $\eta = \frac{2.2}{1.2} = 1.83$, $\xi = 2.40$.

The resulting values of $F^{\frac{1}{\gamma}}$ are,

on the subsonic side of the slip stream where $\rho = 1.8$: $F^{\frac{1}{\gamma}} = \frac{(9.08)^{5/7}}{3.66} = 1.320$

on the supersonic side of the slip stream where $\rho = 2.4$: $F^{\frac{1}{\gamma}} = 1.028$.

The ratio of the $F^{\frac{1}{\gamma}}$ values is 1.320/1.028 = 1.29, equal to that of the ρ-values (2.4/1.8 = 1.33) as it should be, since the pressures are the same on both sides.

7. Direct measurement of Mach number with probes - discrepancies with Mach number from density.

Direct measurements of Mach number were made by extending a probe into the jet, and measuring the angle of the head wave appearing on the shadowgrams. (See Part IV, Sec. 2). Figures 19(a) and (b) illustrate two of these shadowgrams.

In Fig. 20 the Mach number values have been located on a much enlarged shadowgram of the 10-S-60 jet. The tail of each arrow is the place of measurement; the number just below is the probe value; the number in parentheses is the Mach number calculated from the density; the stream flow direction is indicated by the direction of the arrow, and also in degrees to right or left of vertical as shown at the arrow head, and is obtained by bisecting the head wave of the probe. A private communication recently received from Dr. Z. Kopal of Massachusetts Institute of Technology shows that in general a cone which is yawed against the stream produces a headwave which is also yawed, but for slender cones the effect is very small, so that the bisector of the cone headwave actually lies along the stream direction, even though the cone axis does not (for a cone of semi-angle 5° at Mach number 1.7 the shock-cone yaw ratio is only 0.02).

The agreement between directly measured and computed Mach numbers is reasonably good near the orifice, but becomes progressively worse near the shock regions. Those directly measured values enclosed in boxes differ greatly from those computed, and an inspection of the associated shadowgrams (Figs. 19(b) and (d) shows evidence of a strong shock line

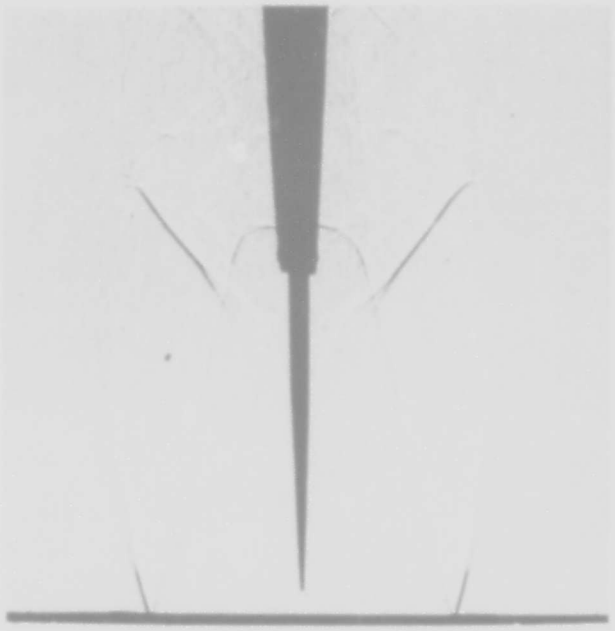

(a)

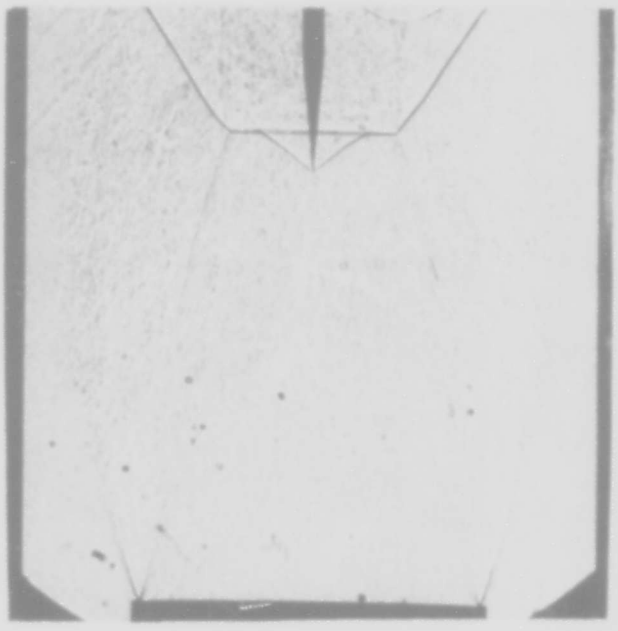

(b)

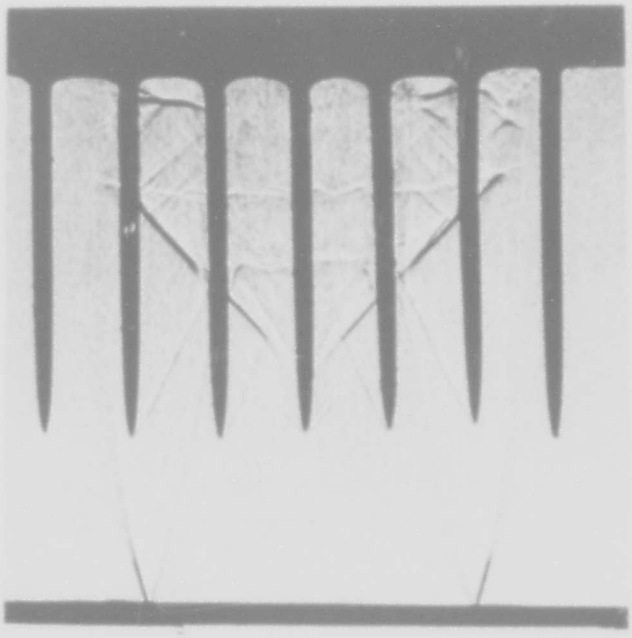

(c)

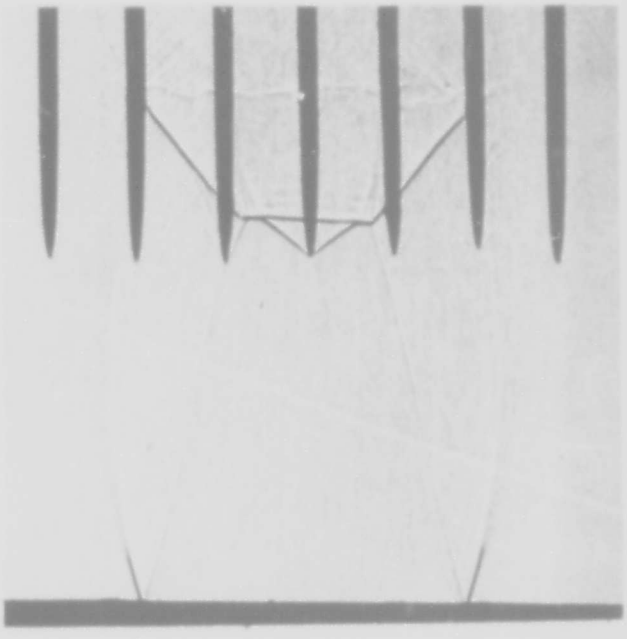

(d)

Fig. 19. 10-S-60 jet with probe for measuring Mach numbers.

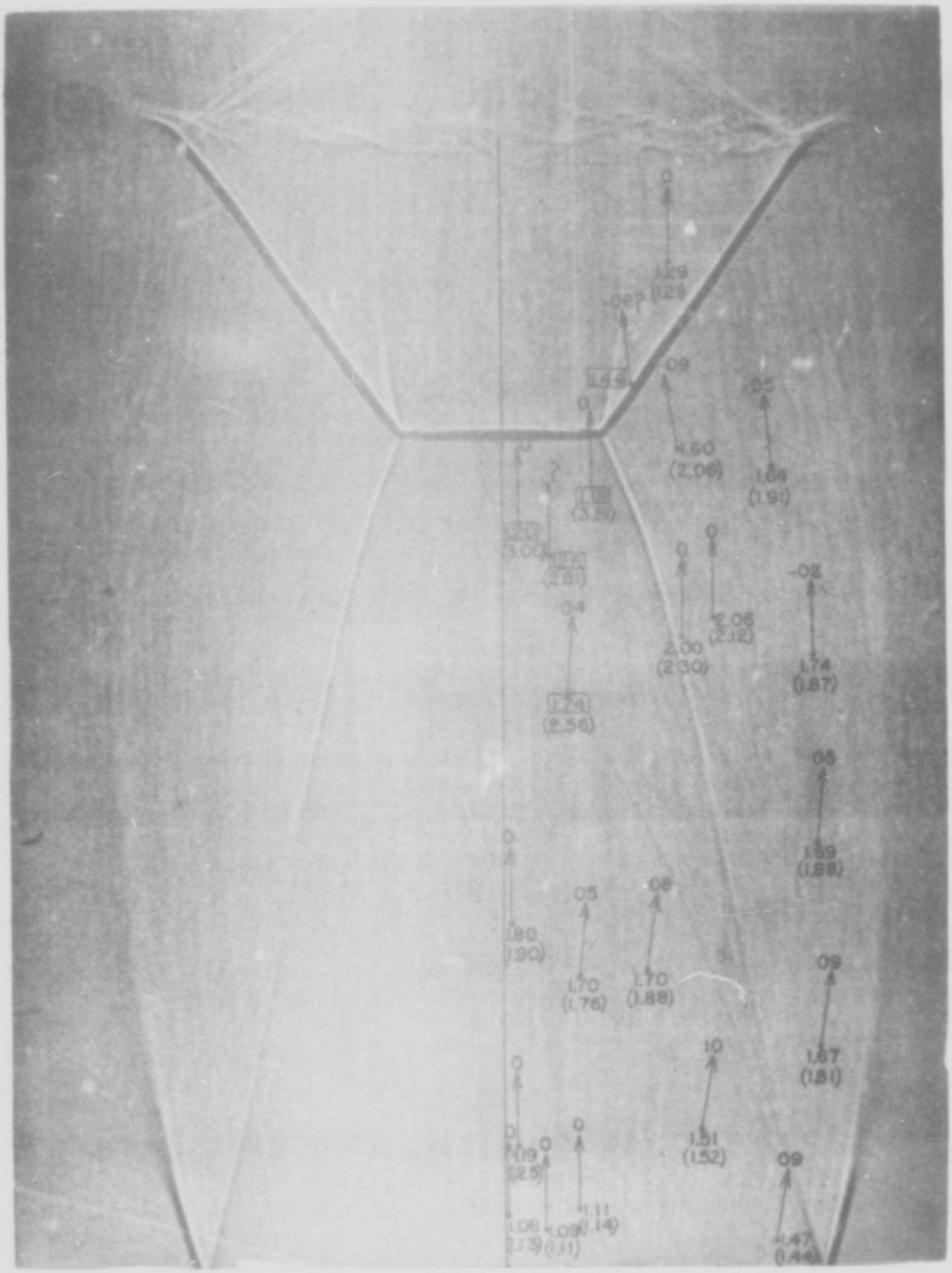

Fig. 20 Mach number distribution in the 10-S-60 jet

from the needle point when just below shock 2, while near the orifice (Figs. 19(a) and (c)) the needle shock appears weak, as would be expected from such a small cone. The multiple probe of Fig. 19 (C) and (D) gives qualitative results only, as the points have not been specially ground. The 2° cone (19-A) or the 10° cone (19-B) give quantitative values. The natural jet turbulence appears in (19-B) as this photograph was made with a spark of 1 μsec., while (19-A, C, and D) were made with a longer duration source (Part III 5-iii).

A separate investigation has been undertaken to determine the cause of the Mach number discrepancy described above; a complete account of the results will be given in a separate report. Interferometric and shadowgraph investigations, with suggestions derived from the literature and other experiments, show that the subsonic boundary layer which develops along the probe produces a conical "dead water" region and a violent divergence of the stream in the neighborhood of a normal shock, and this divergence (compression) occurs through a strong oblique shock wave, which appears about the needle point like a head wave. Due to its large amplitude, the shock occurs at an angle α much larger than the local Mach angle, and the application of the simple relation $M = 1/\sin\alpha$ to it then gives far too low a Mach number. The discrepancy between observed and computed Mach numbers is thus explained. This effect completely changes the structure of the jet downstream from the probe headwave when the probe is inserted (see Fig. 19),

but conditions on the upstream side remain unchanged. This boundary layer phenomenon undoubtedly explains why Cranz and Glatzel (11) apparently found that the Mach number at first increased, but then decreased at greater distances from the orifice, near the normal Mach shock region. Furthermore, Cranz and Glatzel show roughly the direction of the streamlines in the jet, and the continuous expansion is incompatible with a decreasing Mach number out from the orifice.

8. Moving film records of the 10-S-60 jet

It has been found possible to record the position of the interference fringes as a continuous function of time by focusing them with vertical orientation on a fine horizontal slit placed just before the film of a 35 mm high speed recording camera. The film is made to run vertically in a continuous manner with a speed of about one cm/milli-sec., so that the points of light formed where the bright fringes intersect the slit are drawn out into traces, which show a sidewise displacement if the fringes shift. The slit opening corresponds to approximately 20 μsec. In this way one cross section in the jet may be explored at a time, for example, the section near the orifice whose moving film record is shown in Figure 21. This shows the presence of a regular oscillation of the fringes, corresponding to a frequency of about 8000 cycles/sec., which is probably associated with standing sound waves in the orifice. This may be a partial explanation of the fact that Hartman (20) was able to produce ultra-sonic sound vibrations by projecting

BLANK PAGE

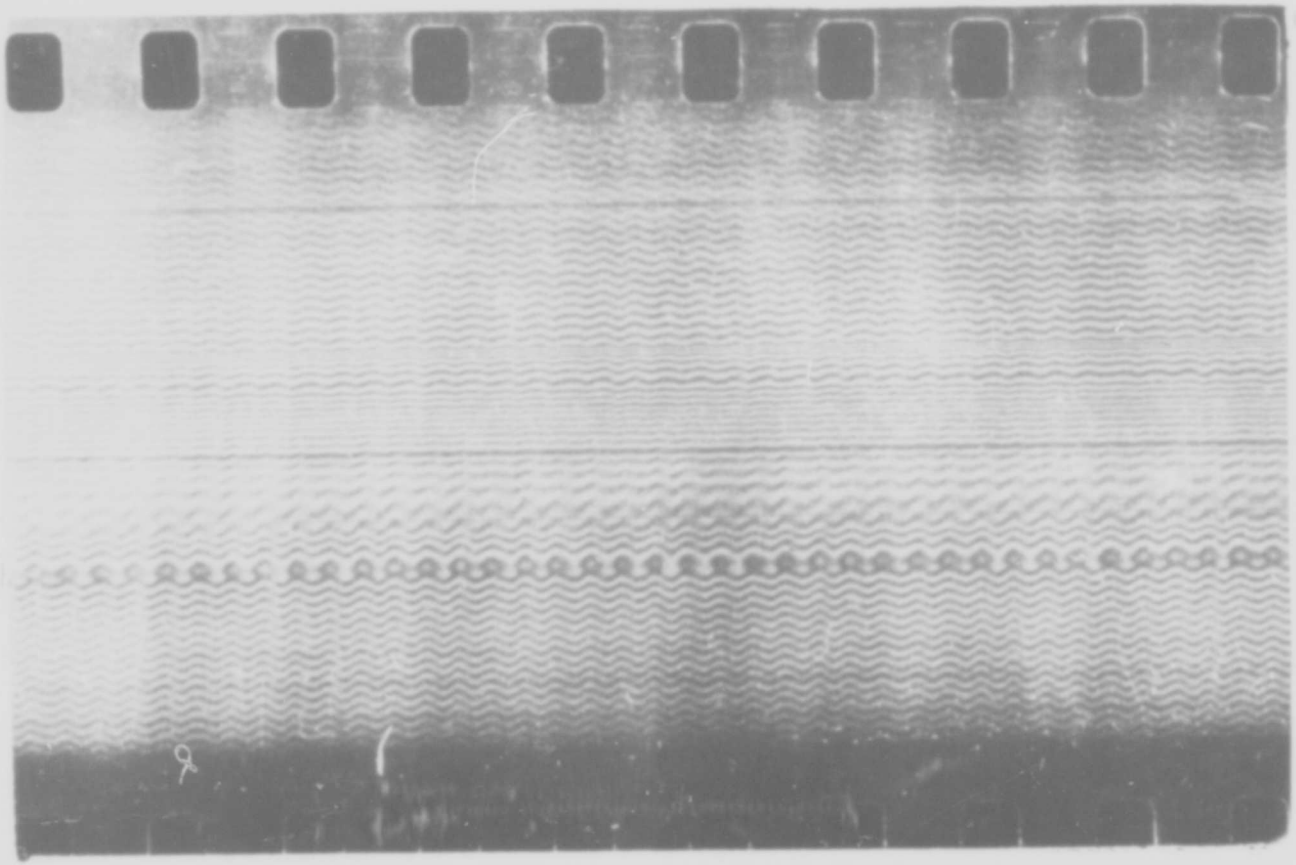

Traces of Fringes
Jet On

Undisplaced Fringes
Jet Off

Fig. 21
Moving Film Records of the 10-S-60 Jet

such an air jet against a suitable resonator.

It is believed that the jet is quasi-stationary with respect to these oscillations as their time of propagation across the jet is much shorter than their period, and that they do not introduce any serious errors due to averaging during the exposure (≈ 300 μsec or ≈ 3 cycles).

BLANK PAGE

A

APPENDIX

MASTER TABLE FOR CALCULATIONS BY ZONE METHOD

VAN VOORHIS-WEYL FORMULATION

μ \ i	0	1	2	3	4	5	6	7	8	9	10	11	12	13	14	15	16	17	18	19	20	21	22	23	24	25	26	27	28	29	30	31	32	33	34	35	36	37	38	39	
0	1.
1	2.	2.1471
2	2.	2.4283	2.8585
3	2.	2.1306	2.8716	3.4247
4	2.	2.0680	2.3270	3.2631	3.9096
5	2.	2.0421	2.1874	2.5234	3.6147	4.3407
6	2.	2.0288	2.1235	2.3174	2.7125	3.9361	4.7326
7	2.	2.0208	2.0680	2.2168	2.4464	2.8915	4.2337	5.0945
8	2.	2.0159	2.0662	2.1592	2.3136	2.5730	3.0615	4.5119	5.4322
9	2.	2.0125	2.0516	2.1223	2.2346	2.4103	2.6957	3.2233	4.7741	5.7502
10	2.	2.0102	2.0415	2.0971	2.1835	2.3120	2.5056	2.8142	3.3780	5.0227	6.0515
11	2.	2.0084	2.0340	2.0792	2.1479	2.2470	2.3893	2.5990	2.9288	3.5263	5.2596	6.3384
12	2.	2.0070	2.0285	2.0656	2.1219	2.2011	2.3112	2.4657	2.6901	3.0398	3.6690	5.4866	6.6130
13	2.	2.0060	2.0241	2.0554	2.1024	2.1674	2.2556	2.3755	2.5411	2.7769	3.1471	3.8062	5.7047	6.8767
14	2.	2.0052	2.0207	2.0475	2.0871	2.1416	2.2144	2.3107	2.4394	2.6151	2.8656	3.2512	3.9389	5.9141	7.1304
15	2.	2.0045	2.0180	2.0412	2.0752	2.1216	2.1827	2.2623	2.3658	2.5025	2.6876	2.9501	3.3523	4.0676	6.1170	7.3756
16	2.	2.0039	2.0158	2.0361	2.0660	2.1057	2.1579	2.2248	2.3104	2.4205	2.5647	2.7587	3.0326	3.4506	4.1921	6.3132	7.6129
17	2.	2.0035	2.0140	2.0319	2.0579	2.0928	2.1379	2.1982	2.2674	2.3586	2.4748	2.6261	2.8284	3.1130	3.5462	4.3132	6.5034	7.8429
18	2.	2.0031	2.0125	2.0284	2.0513	2.0821	2.1216	2.1721	2.2331	2.3102	2.4066	2.5285	2.6863	2.8967	3.1919	3.6396	4.4312	6.6861	8.0663
19	2.	2.0028	2.0112	2.0254	2.0458	2.0732	2.1080	2.1515	2.2054	2.2715	2.3530	2.4544	2.5816	2.7456	2.9636	3.2686	3.7306	4.5461	6.8681	8.2837
20	2.	2.0025	2.0101	2.0229	2.0413	2.0657	2.0967	2.1353	2.1825	2.2400	2.3101	2.3956	2.5014	2.6340	2.8039	3.0295	3.3438	3.8198	4.6582	7.0435	8.4958
21	2.	2.0023	2.0092	2.0207	2.0374	2.0593	2.0871	2.1215	2.1633	2.2140	2.2749	2.3486	2.4381	2.5480	2.6857	2.8610	3.0938	3.4174	3.9067	4.7675	7.2144	8.7025
22	2.	2.0021	2.0083	2.0189	2.0340	2.0538	2.0789	2.1098	2.1472	2.1921	2.2457	2.3099	2.3869	2.4802	2.5942	2.7365	2.9174	3.1568	3.4896	3.9921	4.8748	7.3818	8.9044
23	2.	2.0019	2.0076	2.0173	2.0310	2.0491	2.0718	2.0997	2.1333	2.1734	2.2212	2.2778	2.3449	2.4252	2.5219	2.6397	2.7866	2.9733	3.2191	3.5605	4.0753	4.9791	7.5452	9.1019
24	2.	2.0017	2.0070	2.0159	2.0283	2.0449	2.0657	2.0910	2.1215	2.1577	2.2003	2.2506	2.3099	2.3799	2.4632	2.5633	2.6850	2.8357	3.0275	3.2800	3.6299	4.1565	5.0818	7.7051	9.2953
25	2.	2.0016	2.0064	2.0146	2.0259	2.0413	2.0603	2.0834	2.1111	2.1439	2.1824	2.2276	2.2801	2.3420	2.4148	2.5008	2.6041	2.7296	2.8847	3.0812	3.3401	3.6985	4.2368	5.[illegible]	7.8617	9.4845
26	2.	2.0015	2.0059	2.0134	2.0239	2.0381	2.0555	2.0767	2.1022	2.1320	2.1669	2.2073	2.2549	2.3098	2.3739	2.4493	2.5381	2.6446	2.7732	2.9327	3.1342	3.3990	3.7651	4.3163	5.2812	8.0149	9.6701
27	2.	2.0014	2.0054	2.0124	2.0223	2.0352	2.0513	2.0709	2.0941	2.1215	2.1533	2.1903	2.2328	2.2821	2.3396	2.4061	2.4838	2.5751	2.6847	2.8169	2.9798	3.1864	3.4571	3.831[illegible]	4.3936	5.3780	8.1663	9.8522
28	2.	2.0013	2.0061	2.0115	2.0207	2.0327	2.0476	2.0656	2.0870	2.1121	2.1413	2.1749	2.2139	2.2583	2.3095	2.3592	2.4375	2.5180	2.6121	2.7240	2.8598	3.0266	3.2377	3.5142	3.8960	4.4695	5.4732	8.3143	10.0311
29	2.	2.0012	2.0048	2.0107	2.0193	2.0304	2.0442	2.0610	2.0808	2.1039	2.1308	2.1617	2.1970	2.2377	2.2840	2.3372	2.3984	2.4691	2.5518	2.6486	2.7631	2.9019	3.0727	3.2879	3.5706	3.9599	4.5443	5.5668	8.4598	10.2068
30	2.	2.0011	2.0045	2.0100	2.0180	2.0285	2.0413	2.0568	2.0752	2.0967	2.1214	2.1498	2.1823	2.2194	2.2617	2.3096	2.3649	2.4276	2.5005	2.5851	2.6845	2.8022	2.9436	3.1160	3.3377	3.6263	4.0227	4.6179	5.6587	8.6027	10.3794
31	2.	2.0010	2.0042	2.0094	2.0170	2.0266	2.0386	2.0531	2.0702	2.0901	2.1130	2.1394	2.1692	2.2031	2.2417	2.2856	2.3354	2.3922	2.4568	2.5319	2.6165	2.7200	2.8403	2.9852	3.1630	3.3866	3.6806	4.0845	4.6904	5.7493	8.7434	10.5494
32	2.	2.0010	2.0040	2.0089	2.0159	2.0249	2.0361	2.0497	2.0656	2.0841	2.1055	2.1297	2.1576	2.1890	2.2245	2.2643	2.3094	2.3608	2.4195	2.4859	2.5625	2.6513	2.7556	2.8780	3.0259	3.2072	3.4353	3.7343	4.1455	4.7618	5.8384	8.8816	10.7165
33	2.	2.0009	2.0038	2.0084	2.0149	2.0234	2.0339	2.0466	2.0615	2.0789	2.0987	2.1214	2.1471	2.1760	2.2088	2.2456	2.2873	2.3338	2.3866	2.4465	2.5150	2.5934	2.6840	2.7904	2.9158	3.0662	3.2509	3.4833	3.7872	4.2055	4.8321	5.9263	9.0182	10.8612
34	2.	2.0009	2.0036	2.0079	2.0140	2.0220	2.0319	2.0437	2.0578	2.0740	2.0926	2.1138	2.1376	2.1647	2.1948	2.2288	2.2667	2.3095	2.3576	2.4121	2.4736	2.5438	2.6239	2.7168	2.8247	2.9526	3.1061	3.2941	3.5307	3.8396	4.2649	4.9014	6.0129	9.1524	11.0434
35	2.	2.0008	2.0034	2.0075	2.0132	2.0207	2.0301	2.0412	2.0544	2.0696	2.0870	2.1068	2.1291	2.1541	2.1822	2.2136	2.2489	2.2882	2.3325	2.3816	2.4376	2.5000	2.5719	2.6541	2.7486	2.8590	2.9891	3.1454	3.3367	3.5773	3.8912	4.3234	4.9696	6.0981	9.2848	11.2031
36	2.	2.0008	2.0032	2.0071	2.0124	2.0195	2.0284	2.0389	2.0513	2.0656	2.0820	2.1006	2.1214	2.1448	2.1708	2.2003	2.2327	2.2692	2.3097	2.3551	2.4055	2.4627	2.5272	2.6002	2.6839	2.7805	2.8929	3.0254	3.1844	3.3789	3.6234	3.9423	4.3811	5.0372	6.1823	9.4153	11.3608
37	2.	2.0007	2.0030	2.0067	2.0117	2.0185	2.0268	2.0368	2.0485	2.0620	2.0774	2.0948	2.1144	2.1364	2.1607	2.1878	2.2184	2.2518	2.2891	2.3309	2.3775	2.4298	2.4881	2.5534	2.6285	2.7136	2.8120	2.9264	3.0613	3.2229	3.4205	3.6689	3.9927	4.4379	5.1036	6.2653	9.5438	11.5162
38	2.	2.0007	2.0029	2.0063	2.0111	2.0176	2.0254	2.0348	2.0459	2.0586	2.0730	2.0895	2.1080	2.1285	2.1515	2.1770	2.2051	2.2367	2.2713	2.3096	2.3523	2.4000	2.4532	2.5134	2.5803	2.6562	2.7432	2.8433	2.9597	3.0967	3.2610	3.4617	3.7138	4.0425	4.4942	5.1694	6.3473	9.6709	11.6695
39	2.	2.0007	2.0028	2.0060	2.0106	2.0167	2.0241	2.0330	2.0435	2.0555	2.0692	2.0847	2.1021	2.1212	2.1430	2.1667	2.1932	2.2222	2.2546	2.2905	2.3301	2.3733	2.4225	2.4768	2.5379	2.6069	2.6839	2.7724	2.8742	2.9926	3.1318	3.2967	3.5024	3.7583	4.0917	4.5499	5.2344	6.4281	9.7962	11.8209
40	2.	2.0006	2.0027	2.0057	2.0101	2.0158	2.0229	2.0314	2.0413	2.0527	2.0657	2.0803	2.0966	2.1148	2.1350	2.1575	2.1823	2.2093	2.2397	2.2728	2.3095	2.3501	2.3947	2.4449	2.5004	2.5619	2.6324	2.7113	2.8014	2.9048	3.0252	3.1666	3.3358	3.5427	3.8023	4.1403	4.6047	5.2985	6.5080	9.9199	11.[illegible]
41	2.	2.0006	2.0026	2.0054	2.0096	2.0150	2.0218	2.0298	2.0392	2.0500	2.0623	2.0762	2.0916	2.1089	2.1280	2.1490	2.1723	2.1981	2.2260	2.2570	2.2912	2.3289	2.3703	2.4157	2.4668	2.5237	2.5870	2.6580	2.7386	2.8301	2.9352	3.0573	3.2011	3.3728	3.5825	3.8457	4.1883	4.6590	5.3620	6.5870	10.0[illegible]
42	2.	2.0006	2.0025	2.0051	2.0091	2.0143	2.0207	2.0283	2.0373	2.0475	2.0592	2.0723	2.0871	2.1033	2.1214	2.1413	2.1631	2.1871	2.2136	2.2426	2.2744	2.3096	2.3481	2.3907	2.4374	2.4892	2.5470	2.6116	2.6857	2.7656	2.8586	2.9655	3.0893	3.2351	3.4093	3.6220	3.8887	4.2359	4.7126	5.4245	6.6[illegible]
43	2.	2.0006	2.0024	2.0048	2.0087	2.0137	2.0197	2.0270	2.0355	2.0453	2.0564	2.0687	2.0828	2.0981	2.1152	2.1342	2.1549	2.1775	2.2023	2.2294	2.2594	2.2919	2.3281	2.3671	2.4103	2.4584	2.5113	2.5702	2.6358	2.7093	2.7924	2.8868	2.9953	3.1210	3.2689	3.4454	3.6610	3.9313	4.2828	4.7656	5.4[illegible]
44	2.	2.0005	2.0023	2.0046	2.0083	2.0131	2.0189	2.0258	2.0338	2.0432	2.0537	2.0654	2.0788	2.0934	2.1097	2.1274	2.1470	2.1684	2.1917	2.2175	2.2450	2.2762	2.3095	2.3462	2.3864	2.4306	2.4794	2.5333	2.5932	2.6599	2.7346	2.8190	2.9149	3.0248	3.1524	3.3023	3.4813	3.6995	3.9734	4.3294	4.8[illegible]
45	2.	2.0005	2.0022	2.0044	2.0079	2.0125	2.0181	2.0246	2.0323	2.0413	2.0513	2.0625	2.0751	2.0891	2.1044	2.1212	2.1399	2.1603	2.1822	2.2065	2.2328	2.2614	2.2922	2.3273	2.3649	2.4056	2.4506	2.5002	2.5551	2.6159	2.6837	2.7597	2.8454	2.9427	3.0542	3.1835	3.3354	3.5165	3.7378	4.0149	4.7[illegible]
46	2.	2.0005	2.0021	2.0042	2.0076	2.0120	2.0173	2.0236	2.0309	2.0394	2.0490	2.0598	2.0717	2.0850	2.0996	2.1154	2.1333	2.1523	2.1733	2.1962	2.2209	2.2480	2.2760	2.3092	2.3444	2.3827	2.4246	2.4705	2.5210	2.5769	2.6386	2.7075	2.7847	2.8715	2.9702	3.0834	3.2144	3.3683	3.5518	3.7757	4.0[illegible]
47	2.	2.0005	2.0020	2.0040	2.0073	2.0115	2.0165	2.0226	2.0296	2.0377	2.0469	2.0572	2.0686	2.0812	2.0951	2.1103	2.1270	2.1453	2.1651	2.1867	2.2102	2.2357	2.2632	2.2939	2.3259	2.3621	2.4011	2.4437	2.4904	2.5418	2.5985	2.6613	2.7311	2.8094	2.8976	2.9975	3.1121	3.2449	3.4007	3.5866	3.8[illegible]
48	2.	2.0005	2.0019	2.0038	2.0070	2.0110	2.0158	2.0216	2.0284	2.0360	2.0449	2.0547	2.0657	2.0777	2.0909	2.1054	2.1212	2.1388	2.1574	2.1777	2.2000	2.2241	2.2503	2.2791	2.3097	2.3429	2.3795	2.4192	2.4626	2.5101	2.5623	2.6200	2.6837	2.7546	2.8340	2.9234	3.0247	3.1407	3.2751	3.4329	3.6[illegible]
49	2.	2.0004	2.0018	2.0036	2.0067	2.0106	2.0151	2.0207	2.0272	2.0345	2.0430	2.0524	2.0629	2.0744	2.0870	2.1008	2.1159	2.1325	2.1503	2.1694	2.1910	2.2138	2.2385	2.2654	2.2942	2.3255	2.3596	2.3968	2.4372	2.4815	2.5297	2.5828	2.6413	2.7060	2.7779	2.8583	2.9489	3.0516	3.1691	3.3052	3.[illegible]
50	2.	2.0004	2.0017	2.0034	2.0064	2.0101	2.0144	2.0198	2.0261	2.0330	2.0412	2.0501	2.0602	2.0713	2.0834	2.0964	2.1109	2.1266	2.1436	2.1616	2.1814	2.2036	2.2272	2.2527	2.2797	2.3096	2.3416	2.3763	2.4142	2.4553	2.5003	2.5494	2.6032	2.6625	2.7282	2.8011	2.8826	2.9744	3.0783	3.1973	3.[illegible]

APPENDIX

MASTER TABLE FOR CALCULATIONS BY ZONE METHOD

VAN VOORHIS-WEYL FORMULATION

0																																						
7	6.8767																																					
9	5.9141	7.1304																																				
23	4.0676	6.1170	7.3756																																			
26	3.4506	4.1921	6.3132	7.6129																																		
4	3.1130	3.5462	4.3132	6.5034	7.8429																																	
33	2.8967	3.1919	3.6396	4.4312	6.6861	8.0663																																
6	2.7456	2.9636	3.2686	3.7306	4.5461	6.8681	8.2837																															
4	2.6340	2.8039	3.0295	3.3438	3.8198	4.6582	7.0435	8.4958																														
1	2.5480	2.6857	2.8610	3.0938	3.4174	3.9067	4.7675	7.2144	8.7025																													
9	2.4802	2.5942	2.7365	2.9174	3.1568	3.4896	3.9921	4.8748	7.3818	8.9044																												
9	2.4252	2.5219	2.6397	2.7866	2.9733	3.2191	3.5605	4.0753	4.9791	7.5452	9.1019																											
9	2.3799	2.4632	2.5633	2.6850	2.8357	3.0275	3.2800	3.6299	4.1565	5.0818	7.7051	9.2953																										
1	2.3420	2.4148	2.5008	2.6041	2.7296	2.8847	3.0812	3.3401	3.6985	4.2368	5.1823	7.8617	9.4845																									
9	2.3098	2.3739	2.4493	2.5381	2.6446	2.7732	2.9327	3.1342	3.3990	3.7651	4.3163	5.2812	8.0149	9.6701																								
8	2.2821	2.3396	2.4061	2.4838	2.5751	2.6847	2.8169	2.9798	3.1864	3.4571	3.8311	4.3936	5.3780	8.1663	9.8522																							
9	2.2583	2.3095	2.3692	2.4375	2.5180	2.6121	2.7240	2.8598	3.0266	3.2377	3.5142	3.8960	4.4695	5.4732	8.3143	10.0311																						
0	2.2377	2.2840	2.3372	2.3984	2.4691	2.5518	2.6486	2.7631	2.9019	3.0727	3.2879	3.5706	3.9599	4.5443	5.5668	8.4598	10.2068																					
3	2.2194	2.2617	2.3096	2.3649	2.4278	2.5005	2.5851	2.6845	2.8022	2.9436	3.1180	3.3377	3.6263	4.0227	4.6179	5.6587	8.6027	10.3794																				
2	2.2031	2.2417	2.2856	2.3354	2.3922	2.4568	2.5319	2.6185	2.7200	2.8403	2.9852	3.1630	3.3868	3.6806	4.0845	4.6904	5.7493	8.7434	10.5494																			
6	2.1890	2.2245	2.2643	2.3094	2.3608	2.4195	2.4869	2.5625	2.6513	2.7556	2.8780	3.0259	3.2072	3.4353	3.7343	4.1455	4.7618	5.8384	8.8818	10.7165																		
1	2.1760	2.2088	2.2456	2.2873	2.3338	2.3866	2.4465	2.5150	2.5934	2.6840	2.7904	2.9158	3.0662	3.2509	3.4833	3.7872	4.2055	4.8321	5.9263	9.0182	10.8812																	
6	2.1647	2.1948	2.2288	2.2667	2.3095	2.3576	2.4121	2.4736	2.5438	2.6239	2.7168	2.8247	2.9526	3.1061	3.2941	3.5307	3.8596	4.2649	4.9014	6.0129	9.1524	11.0434																
1	2.1541	2.1822	2.2136	2.2489	2.2882	2.3325	2.3816	2.4376	2.5000	2.5719	2.6541	2.7486	2.8590	2.9891	3.1454	3.3367	3.5773	3.8912	4.3234	4.9696	6.0981	9.2848	11.2031															
4	2.1448	2.1708	2.2003	2.2327	2.2692	2.3097	2.3551	2.4055	2.4627	2.5272	2.6002	2.6839	2.7805	2.8929	3.0254	3.1844	3.3789	3.6234	3.9423	4.3811	5.0372	6.1823	9.4153	11.3608														
4	2.1364	2.1607	2.1878	2.2184	2.2518	2.2891	2.3309	2.3775	2.4298	2.4881	2.5534	2.6285	2.7136	2.8120	2.9264	3.0613	3.2229	3.4205	3.6689	3.9927	4.4379	5.1038	6.2653	9.5438	11.5162													
0	2.1285	2.1515	2.1770	2.2051	2.2367	2.2713	2.3096	2.3523	2.4000	2.4532	2.5134	2.5803	2.6562	2.7432	2.8433	2.9597	3.0967	3.2610	3.4617	3.7136	4.0425	4.4942	5.1694	6.3473	9.6709	11.6695												
1	2.1212	2.1430	2.1667	2.1932	2.2222	2.2546	2.2905	2.3301	2.3733	2.4225	2.4768	2.5379	2.6069	2.6839	2.7724	2.8742	2.9926	3.1318	3.2987	3.5024	3.7583	4.0917	4.5499	5.2344	6.4281	9.7962	11.8209											
6	2.1148	2.1350	2.1575	2.1823	2.2093	2.2377	2.2728	2.3095	2.3501	2.3947	2.4449	2.5004	2.5619	2.6324	2.7113	2.8014	2.9048	3.0252	3.1666	3.3358	3.5427	3.8023	4.1403	4.6047	5.2985	6.5080	9.9199	11.9703										
6	2.1089	2.1280	2.1490	2.1723	2.1981	2.2260	2.2570	2.2912	2.3289	2.3703	2.4157	2.4668	2.5237	2.5870	2.6580	2.7386	2.8301	2.9352	3.0573	3.2011	3.3728	3.5825	3.8457	4.1883	4.6590	5.3620	6.5870	10.0422	12.1180									
1	2.1033	2.1214	2.1413	2.1631	2.1871	2.2138	2.2426	2.2744	2.3096	2.3481	2.3907	2.4374	2.4892	2.5470	2.6116	2.6837	2.7656	2.8586	2.9655	3.0893	3.2351	3.4093	3.6220	3.8887	4.2359	4.7126	5.4245	6.6650	10.1628	12.2637								
8	2.0981	2.1152	2.1342	2.1549	2.1775	2.2023	2.2294	2.2594	2.2919	2.3281	2.3671	2.4103	2.4584	2.5113	2.5702	2.6358	2.7093	2.7924	2.8868	2.9953	3.1210	3.2689	3.4454	3.6610	3.9313	4.2828	4.7656	5.4865	6.7420	10.2823	12.4079							
8	2.0934	2.1097	2.1274	2.1470	2.1684	2.1917	2.2175	2.2450	2.2762	2.3095	2.3462	2.3864	2.4306	2.4794	2.5333	2.5932	2.6599	2.7346	2.8190	2.9149	3.0248	3.1524	3.3023	3.4813	3.6995	3.9734	4.3294	4.8181	5.5476	6.8183	10.4003	12.5504						
1	2.0891	2.1044	2.1212	2.1399	2.1603	2.1822	2.2065	2.2328	2.2614	2.2922	2.3273	2.3649	2.4056	2.4506	2.5002	2.5551	2.6159	2.6837	2.[illegible]597	2.8454	2.9427	3.0542	3.1835	3.3354	3.5165	3.7378	4.0149	4.3754	4.8702	5.6081	6.8936	10.5168	12.6912					
7	2.0850	2.0996	2.1154	2.1333	2.1523	2.1733	2.1962	2.2209	2.2480	2.2760	2.3092	2.3444	2.3827	2.4246	2.4705	2.5210	2.5769	2.6366	2.7075	2.7847	2.8715	2.9702	3.0834	3.2144	3.3683	3.5518	3.7757	4.0562	4.4209	4.9214	5.6680	6.9683	10.6324	12.8308				
6	2.0812	2.0951	2.1103	2.1270	2.1453	2.1651	2.1867	2.2102	2.2357	2.2632	2.2939	2.3259	2.3621	2.4011	2.4437	2.4904	2.5418	2.5985	2.6613	2.7311	2.8094	2.8976	2.9975	3.1121	3.2449	3.4007	3.5866	3.8131	4.0971	4.4661	4.9722	5.7273	7.0419	10.7464	12.9683			
7	2.0777	2.0909	2.1054	2.1212	2.1388	2.1574	2.1777	2.2000	2.2241	2.2503	2.2791	2.3097	2.3429	2.3795	2.4192	2.4626	2.5101	2.5623	2.6200	2.6837	2.7546	2.8340	2.9234	3.0247	3.1407	3.2751	3.4329	3.6211	3.8503	4.1375	4.5108	5.0227	5.7859	7.1149	10.8595	13.1048		
9	2.0744	2.0870	2.1008	2.1159	2.1325	2.1503	2.1694	2.1910	2.2138	2.2385	2.2654	2.2942	2.3255	2.3596	2.3968	2.4372	2.4815	2.5297	2.5828	2.6413	2.7060	2.7779	2.8583	2.9489	3.0516	3.1691	3.3052	3.4649	3.6552	3.8872	4.1776	4.5550	5.0728	5.8442	7.1872	10.9711	13.2397	
2	2.0713	2.0834	2.0964	2.1109	2.1266	2.1436	2.1616	2.1814	2.2036	2.2272	2.2527	2.2797	2.3096	2.3416	2.3763	2.4142	2.4553	2.5003	2.5494	2.6032	2.6625	2.7282	2.8011	2.8826	2.9744	3.0783	3.1973	3.3349	3.4965	3.6891	3.9235	4.2171	4.5987	5.1218	5.9017	7.2587	11.0818	13.3733
	13	14	15	16	17	18	19	20	21	22	23	24	25	26	27	28	29	30	31	32	33	34	35	36	37	38	39	40	41	42	43	44	45	46	47	48	49	50

BLANK PAGE

LIST OF REFERENCES

1. St. Venant and Wantzel, Jour. de l'Ecole Polytechnique 16, 85 (1839)

2. A) Ackeret. J. Handbuch der Physik, 7, Chapter 5 "Gasdynamik" Springer, Berlin (1927)

   B) Batemen, H., Bulletin of the National Research Council No. 84, Feb. (1932) Committee on Hydrodynamics, Part 4, "Compressible Fluids".

   C) Aerodynamic Theory, ed. by W. F. Durand Vol. 3, Division H "The Mechanics of Compressible Fluids" G. I. Taylor and J. W. MacColl

3. Reynolds, Osborne, "On the Flow of Gases", Phil. Mag. 21 185-199 March (1886)

4. Mach, E., and Salcher, P., "Optische Untersuchung der Luftstrahlen", Wiener Berichte, 98, 1303-1309, Nov. (1889)

5. Emden, R., "Uber die stationaren Wellen in einem Gasstrahl", Ann. der Physik, 69, 264-269, 426-455 (1899)

6. Prandtl, L., "Uber die stationaren Wellen in einem Gasstrahl", Physik, Zeit., 5, 599-601, (1904)

7. Karman, Th., "Uber die stationaren Wellen in einem Gasstrahl", Physik, Zeit., 8, 209-211, (1907)

8. Rayleigh, Lord, "On the Discharge of Gases Under High Velocity" Phil. Mag., 6, 177-187, (1916)

9. Mach, L., "Optische Untersuchung der Luftstrahlen" Wiener Berichte, 106, 1025-1074, (1897)

10. A) Mach, E., and Wosyka, J. "Uber einige mechanische Wirkungen des elektrischen funkens" Wiener Berichte 72-II, 44-52 (1875)

    B) Rosicky, W., "Uber mechanische - akustische Wirkungen des elektrischen funkens" Wiener Berichte 73-II, 629-650 (1876)

C) Mach, E., and Sommer, J. "Uber die fortpflanzungs geschwindigkeit von Explosions-schallen" Wiener Berichte 75-II 101-130 (1877)

D) Mach, E., Tumlitz, O., and Kogler, C "Über die fortpflanzungs geschwindigkeit der funkenwellen" Wiener Berichte 77-II, 7-32 (1878)

E) Mach, E. "Uber die Verlauf der funkenwellen in der Ebene und im Raume" Wiener Berichte 77-II, 819-838 (1878)

F) Mach, E., and Gruss, G. "Optische Untersuchung der funkenwellen" Wiener Berichte 78-II 467-480 (1878)

G) Mach, E., and Simonides, J. "Weitere Untersuchung der Funkenwellen" Wiener Berichte 80-II 476-486 (1879)

H) Mach, E., and Mach, L. "Uber die Interferenz der Schallwellen von grosser Excursion" Wiener Berichte 98 1333 - 1336 (1889)

11. Cranz, C., and Glatzel, B., "Die Ausstromung von Gasen bei hohen Anfangsdrucken", Ann. der Physik, 43 1186-1204 (1914)

12. Stanton, T. E., "On the Flow of Gases at High Speeds", Proc. Roy. Soc., 111-A, 306-339, (1926)

13. Hartman and Lazarus, "The Air Jet with a Velocity exceeding that of Sound", Phil. Mag., 31, 35-50, (1941)

14. Prandtl, L., "Neue Untersuchung uber die Stromende Bewegung der Gase and Dampfe", Phys. Zeit., 8, 23-30 (1907)

15. Schardin, H., "Das Toeplersche Schlierenverfahren" Forschungsheft 367, 5, July/August, (1934)

16. A) Mach, L., "Uber ein Interferenzrefractometer" Wiener Berichte 101, 5-10, (1892) 102, 1035-1056 (1893)

"Uber einige Verbesserung an Interferenzapparaten" Wiener Berichte 107, 851 - 859 (1898)

BLANK PAGE

B) Zehnder, "Ein neuer Interferenzrefraktor", Zeit. fur Instrumentenkunde, 11, 275-285, (1891)

17. Bibliography of Interferometric Studies of Gas Dynamics

A) Cranz, C., "Lehrbuch der Ballistik", Julius Springer, Berlin, (1926) Vol. II, 193, Vol. III, 271.

B) Hansen, G., "Uber ein Interferometer nach Zehnder-Mach", Zeit. fur Tech. Physik, 12, 436-440 (1931)

C) Kennard, R. B. "Temperature Distribution and Heat Flux in Air by Interferometry" Bureau Stands. Jour. Research, 8, 787-805 (1932)

D) Mach, E., and Weltrubsky, J. "Uber der Formen der Funkenwelle" Wiener Berichte 78, 551 - 560 (1878)

E) Mach, L., "Weitere Versuche uber Projectile" Wiener Berichte 105, 605-635 (1896)

F) Schardin, H., "Theorie and Anwendung des Mach-Zehnderschen Interferenz-Refraktometers", Zeit. fur Instrumentenkunde, 53, Part 1 - 396, Part 2, - 424, (1933)

G) Tremblot, R., "Sur l'etude des courants gazeax au moyen des interferences", Comptes Rendus, 192, 480-482, (1931).

"Sur l'application des interferences a quelques problems d'ecoulement a grands vitesse" Comptes Rendus, 193, 418-419, (1931)

H) Vautier, Th., "Recherches Experimentales sur la propagation d'ondes aeriennes dans un long tuyau cylindrique", Ann. de Phys., 14, 263-626, (1930)

I) Zobel, Th., "Verwendung von Lichtinterferenzen in der Technischen Messung", Zeit. fur Vereines Deut. Ing., 81, 619 (1937)

J) It is known that extensive interferometric studies of gas dynamics have been made before and during World War II in France, and particularly Germany. Reports on this work are very incomplete, and are not available in the general literature.

18. A) Keenan, Ph. C., Explosive Research Report No. 11 (Re2c) "Shadowgraph determination of shock-wave strength". Navy Dept., Bureau of Ordnance, Washington, D.C.

B) Weyl, F. J., NAVORD Report 211-45, "Analytical Methods in Optical Examination of Supersonic Flow", Navy Department, Bureau of Ordnance, Washington, D. C.

19. Taylor and MacColl, "Air Pressure on a Cone Moving at High Speeds", Proc. Roy. Soc., 139, 278-297, 298-311 (1933)

MacColl, "The Conical Shock Wave formed by a Cone moving at High Speed", Proc. Roy. Soc. 159, 459-471, (1937)

20. Hartman, J., "On a New Method for the Generation of Sound Waves", Phys. Rev. 20, 719 (1922)

21. Bibliography of Theory of Shock Waves

A) Poisson, M., "Sur le Theorie du Son" Journal de l'Ecole Polytechnique, Paris 13-14, 319-392 (1808)

B) Stokes, G.G., On a Difficulty in the Theory of Sound Phil. Mag. 33 349 (1848) Math. and Phys. Papers, 2, 51-55

C) Riemann, B., "Uber die Fortpflanzung ebener Luftwellen von endlicher Schwingungsweite" Gott. Ges. d. Wiss, 8, (1860) or Reimann's ges. Werke 2 Aufl. 156

D) Ernshaw, S. "On a new Theoretical determination of the velocity of Sound" Phil. Mag. 19 449-455, 20 37-41 186-192 (1860) Trans. Roy. Soc., London, A 150 133-148 (1860) Brit. Assn. Advancement Science (1860) 2:58-59

E) Rankine, W.J.M. "On the thermodynamic theory of waves of finite longitudinal disturbance". Trans. Roy. Soc., London, A 160 277 (1870) Misc. Sci. Papers, Griffin, London (1881) 530-543

F) Hugoniot, H. "Propagation du Mouvement dans les Corps" Journ. de l'ecole Polytechn. Paris Part 1 57 3-97, (1887) Part 2. 58, 1-125 (1889)

G) Rayleigh, Lord "Aerial Plane Waves of Finite Amplitude" Proc. Roy. Soc. A 84 247-284 (1911)

H) Taylor, G. I., "The Conditions Necessary for Discontinuous Motion in Gases" Proc. Roy. Soc. A 84 371-377 (1911)

I) Becker, R., "Stosswelle und Detonation" Zeit. f. Physik 8 321-362 (1921-22)

J) Thomas, "Note on Becker's Theory of Shock Front" Jour. Chem. Physics 12 449-453 (1944)